

# Analysis and modelling of respiratory metabolism in *Neisseria meningitidis*

Andrew Schofield

PhD

The University of York

Biology

March 2012

## **Abstract**

*N. meningitidis* is capable of respiration in both aerobic and microaerobic environments by reduction of oxygen and nitrite respectively. The respiratory chain and genetic regulation of this system are already well understood, but there are complex interactions between components which make predicting which respiratory path will be used difficult. To predict the respiratory behaviour of *N. meningitidis* I have built a mathematical model using a novel combination of experiments and Bayesian fitting.

# Contents

<b>1</b>	<b>Introduction</b>	<b>9</b>
1.1	Biology of <i>Neisseria meningitidis</i>	9
1.2	Pathogenicity of <i>N. meningitidis</i>	10
1.3	Growth of <i>N. meningitidis</i>	12
1.4	Organisation of the Respiratory Chain of <i>N. meningitidis</i>	12
1.5	Respiratory Enzymes in <i>N. meningitidis</i>	17
1.5.1	Cytochrome <i>cbb</i> <sub>3</sub> oxidase	17
1.5.2	NorB Nitric Oxide Reductase	19
1.5.3	AniA Nitrite Reductase	20
1.6	Respiratory Electron Transporters in <i>N. meningitidis</i>	21
1.6.1	NADH Dehydrogenase	21
1.6.2	Cytochrome <i>bc</i> <sub>1</sub> Complex	21
1.6.3	Cytochromes <i>c</i> <sub>4</sub> , <i>c</i> <sub>x</sub> and <i>c</i> <sub>5</sub>	22
1.6.4	Quinone Pool	24
1.7	Respiration Regulatory Proteins in <i>N. meningitidis</i>	25
1.7.1	NsrR - Nitrite Sensing Repressor Protein	25
1.7.2	FNR - Fumarate and Nitrate Reductase Regulator	25
1.7.3	NarQ/NarP - Nitrite Response Sensor/Regulator	26
1.8	Organisation of Respiratory Chains in Other Bacteria	26
1.8.1	The Respiratory Chain of <i>Paracoccus denitrificans</i>	27
1.8.2	The Respiratory Chain of <i>Escherichia coli</i>	28
1.9	Systems Biology	30
1.10	Modelling	33
1.10.1	Modelling Respiratory Systems	33
1.10.2	Modelling Tools	34
1.11	Aims	35
<b>2</b>	<b>Materials and Methods</b>	<b>36</b>
2.1	<i>Neisseria meningitidis</i> Strains Used in This Work	36
2.2	Culturing <i>Neisseria meningitidis</i>	37
2.2.1	Growth of <i>Neisseria meningitidis</i>	37
2.2.2	Preparation of Antibiotic Selective Media	37
2.2.3	Preparation of Frozen Bacterial Stocks	37
2.2.4	Streaking Plates for OD to CFU Ratio Calculation	38
2.3	Measuring Oxygen Concentration	38
2.3.1	Calibration of Oxygen Electrode	38
2.4	Measuring Nitric Oxide Concentration	39
2.4.1	Calibration of Nitric Oxide Electrode	39

2.5	Measuring Nitrite Concentration (Griess Assay)	40
2.6	Nitric Oxide Production	40
<b>3</b>	<b>Model - Construction and Parameters</b>	<b>43</b>
3.1	Construction	43
3.1.1	Converting Biological Reactions into Differential Equations	43
3.1.2	Assumptions and their Justifications	48
3.2	Parameters and their Prior Distributions	49
3.3	Solving Ordinary Differential Equations	55
3.4	Parameter Estimation	56
<b>4</b>	<b>Parameter Estimation Methodologies</b>	<b>57</b>
4.1	Simulated Annealing	58
4.2	Approximate Bayesian Computation by Sequential Monte Carlo	62
4.3	Metropolis Hastings Monte Carlo	66
4.4	Implementation	68
4.5	Integrative Scheme	70
<b>5</b>	<b>Oxygen Reduction in <i>N. meningitidis</i></b>	<b>71</b>
5.1	Aerobic Reduction of Oxygen	71
5.1.1	Introduction	73
5.1.2	Results	73
5.1.3	Discussion	73
<b>6</b>	<b>Nitric Oxide Reduction in <i>N. meningitidis</i></b>	<b>74</b>
6.1	Aerobic Nitric Oxide Reduction	77
6.1.1	Introduction	77
6.1.2	Results	77
6.1.3	Discussion	77
6.2	Microaerobic Nitric Oxide Reduction	77
6.2.1	Introduction	77
6.2.2	Results	77
6.2.3	Discussion	77
6.3	Aerobic Nitric Oxide Reduction in <i>nsrR</i> <sup>-</sup> mutant	77
6.3.1	Introduction	77
6.3.2	Results	77
6.3.3	Discussion	77
<b>7</b>	<b>Nitrite Reduction in <i>N. meningitidis</i></b>	<b>78</b>
7.1	Microaerobic Nitrite Reduction	80
7.1.1	Introduction	80
7.1.2	Results	80
7.1.3	Discussion	80
7.2	Microaerobic Nitrite Reduction in <i>norB</i> <sup>-</sup> mutant	80
7.2.1	Introduction	80
7.2.2	Results	80
7.2.3	Discussion	80
7.3	Aerobic Nitrite Reduction in <i>nsrR</i> <sup>-</sup> mutant	80
7.3.1	Introduction	80

---

7.3.2	Results . . . . .	80
7.3.3	Discussion . . . . .	80
7.4	Aerobic Nitrite Reduction in <i>nsrR<sup>-</sup>-norB<sup>-</sup></i> mutant . . . . .	80
7.4.1	Introduction . . . . .	80
7.4.2	Results . . . . .	80
7.4.3	Discussion . . . . .	80
<b>8</b>	<b>AniA and NorB Expression in <i>N. meningitidis</i></b>	<b>81</b>
8.1	Aerobic and Microaerobic Expression . . . . .	81
8.1.1	Introduction . . . . .	81
8.1.2	Results . . . . .	81
8.1.3	Discussion . . . . .	81
<b>9</b>	<b>The Completed Model</b>	<b>82</b>
<b>A</b>	<b>Appendix</b>	<b>83</b>
	<b>List of Abbreviations</b>	<b>85</b>
	<b>References</b>	<b>85</b>

# List of Figures

1.1	Complete denitrification. . . . .	13
1.2	Layout of the components of the respiratory system in <i>Neisseria meningitidis</i> . . . . .	15
1.3	Regulation of respiratory components in <i>Neisseria meningitidis</i> . . . .	17
1.4	The <i>cbb<sub>3</sub></i> oxidase. . . . .	18
1.5	The modified Q-cycle used by the bacterial <i>bc<sub>1</sub></i> complex. . . . .	23
1.6	Structure of the ubiquinone molecule. . . . .	24
1.7	Branched electron transport chains of <i>N. meningitidis</i> . . . . .	27
1.8	Branched electron transport chains of <i>Paracoccus</i> species. . . . .	28
1.9	Branched electron transport chains of <i>E. coli</i> . . . . .	29
1.10	Systems biology cycle. . . . .	31
1.11	System complexity. . . . .	32
2.1	NO making apparatus. . . . .	41
4.1	Pseudo-code showing how the simplest annealing algorithm works. . . .	59
4.2	Example simulated annealing temperature schedule . . . . .	60
4.3	Schematic diagram showing the technique used to generate a spread of parameters using a synthetic chromosome. . . . .	61
4.4	Simulation results of the Lotka-Volterra validation run. . . . .	68
4.5	MHMC results of the Lotka-Volterra validation run. . . . .	69
5.1	Oxygen Reduction in <i>Neisseria meningitidis</i> . . . . .	72
6.1	Nitric Oxide Reduction in <i>Neisseria meningitidis</i> . . . . .	76
7.1	Nitrite Reduction in <i>Neisseria meningitidis</i> . . . . .	79

# List of Tables

1.1	The reductions catalysed by the respiratory enzymes in <i>N. meningitidis</i> . . . . .	14
2.1	Bacterial strains and sources . . . . .	36
2.2	Final antibiotic concentrations . . . . .	37
2.3	Sodium Nitrite concentrations used to calibrate ISO-NOP Nitric Oxide sensor. . . . .	40
2.4	Chemicals needed for preparation of Nitric Oxide solution. . . . .	41
3.1	Model parameters . . . . .	50
A.1	Model Variables . . . . .	84
A.2	Model Parameters . . . . .	84

# Acknowledgements



# Chapter 1

## Introduction

### 1.1 Biology of *Neisseria meningitidis*

*Neisseria meningitidis* is a Gram-negative, bean-shaped diplococcal bacteria<sup>1</sup>, surrounded by a lipid membrane containing outer membrane proteins and lipopolysaccharides<sup>1</sup>. When pathogenic, the bacteria also has a polysaccharide capsule attached to the membrane<sup>1</sup>. It is non-spore forming, non-motile but piliated, and lives as an obligate human pathogen (humans being its only host)<sup>2</sup>. *N. meningitidis* inhabits the mucosal membranes primarily in the respiratory tract, and it is estimated that up to 20-25% of the population have this bacteria in their nasopharynx while being asymptomatic<sup>2-4</sup>.

The *Neisseria* genus contains a number of non-pathogenic species which are part of the normal human flora including *N. subflava*, *N. flavescens*, *N. lactamica* and *N. sicca*<sup>5</sup>. Two species of *Neisseria* are the causative agents of human diseases, *N. meningitidis*, which causes bacterial meningitis and *N. gonorrhoea* which causes gonorrhoea. Being  $\beta$ -proteobacteria<sup>2</sup>, the *Neisseria* genus is also related to a number of other pathogenic bacteria including *Bordetella* and *Burkholderia*. This taxa also includes nitrogen-fixing bacteria such as *Nitrosomonas*<sup>6</sup>.

*N. meningitidis* is classified into 13 different serogroups based on the differences in lipopolysaccharides, capsules, outer membrane proteins and adhesion molecules<sup>1,2,7</sup>. 3 of these 13 serogroups are the main cause of meningococcal

meningitis, with serogroups B and C being the most prevalent<sup>1</sup>. Vaccines for serogroup C are available, but serogroup B currently has no effective vaccine, as it mimics human antigens<sup>2</sup>. In addition to being the causative agent for meningococcal meningitis, *N. meningitidis* also causes septicaemia and the combination has a mortality rate of 10%<sup>1,2</sup>.

*N. meningitidis* is dependent on a source of iron, and must source this from its environment<sup>8</sup>. It does this by directly capturing iron from the host via human transferrins<sup>8-10</sup> and lactoferrin<sup>8</sup>. This capture is brought about by membrane surface receptors that can bind the transferrins which then go on to internalise the iron into the bacterium for growth<sup>11</sup>.

## 1.2 Pathogenicity of *N. meningitidis*

Meningitis is caused by *N. meningitidis* entering the bloodstream and travelling to the meninges, a set of membranes that envelope the central nervous system, where the bacteria goes on to cause inflammation. Once it has entered the bloodstream, *N. meningitidis* is capable of switching its capsule by phase-variation to avoid host-immune detection<sup>12,13</sup>. After colonisation by the bacterium, in order to enter the bloodstream, it must first adhere to the mucosal tissue. This is facilitated by adhesion molecules on the outer membrane and by pili, with the latter being the primary source of adhesion<sup>1,7</sup>. Once the bacteria are adhered to the mucosal cells, additional contacts are made with the outer membrane proteins. Interestingly, the presence of the polysaccharide capsule, which is required for survival in the bloodstream, interferes with these additional contacts<sup>2</sup>. *N. meningitidis* invades the bloodstream by being endocytosed by the mucosal epithelial cells, a process which is triggered by the pili and outer membrane proteins on the bacteria.

*N. meningitidis* is able to survive in the bloodstream (typically an antimicrobial environment) mainly by virtue of its polysaccharide capsule as this is able to protect the bacteria against various immune responses by the host including

complement-mediated bacteriolysis and phagocytosis by neutrophils<sup>1</sup>. Despite these protective features, specific antibodies *do* provide full protection against the bacteria, but the time taken for these antibodies to be produced means that the host has a period of at least 1 week in which it must rely on innate immune response<sup>1</sup>. Evidence suggests that systemic infection by *N. meningitidis* can only occur in hosts which are immunocompromised in some way, specifically if they do not have the serum bactericidal antibodies against capsular or non-capsular antigens, or they are missing certain complement components<sup>4</sup>. A number of factors can increase the likelihood of contracting bacterial meningitis including smoking and travelling to epidemic regions<sup>2</sup>. In developed countries, the highest rates of invasive meningococcal meningitis are seen in infants and children less than 4 years-old, adolescents, military recruits and groups where crowding and new exposures occur such as college students living in dormitories, however the disease is capable of affecting all age groups<sup>2</sup>.

There is evidence to suggest that much of the damage done to the host during a meningococcal infection is actually caused by the host in an attempt to rid itself of the bacteria<sup>14</sup>. A systemic infection causes a massive inflammatory response and the resulting quantities of cytokines produced eventually lead to organ dysfunction and the proteases produced by neutrophil activation also lead to endothelial injury<sup>14</sup>.

Once *N. meningitidis* has entered the bloodstream, it goes on to invade the cerebro-spinal fluid (CSF), which serves as an excellent culture medium for the bacteria<sup>4</sup>. The host response to this infection is inflammation of the meninges, the membranes surrounding the central nervous system. This leads to a build-up of serous fluid in the brain causing cerebral swelling. Once the bacteria have entered the CSF, antimicrobial treatment is required otherwise the effects are almost invariably fatal<sup>4</sup>.

Initially a meningococcal infection presents as a slight fever and chills, which may improve after 4-6 hours. Haemorrhagic skin lesions may appear between

8 and 18 hours, however roughly 20% of suffers never present with lesions. These skin lesions are possibly the most well known symptom of bacterial meningitis as they are characterised by a non-blanching (does not turn white under mild pressure) rash. The clearest evidence for meningococcal infection is a fever, stiff neck, aversion to bright light, vomiting, skin lesions and headaches. Unfortunately not all these symptoms may be present in all cases<sup>4</sup>.

When meningococcal septicaemia occurs, renal function may be impaired as a direct consequence of cardiac impairment. Septicaemia causes “capillary leak” which reduces cardiac output and increases the effort required to breathe normally. Reduced cardiac output can also affect the gastrointestinal tract leading to reduced function. Once treated these symptoms will usually subside as cardiac output improves<sup>14</sup>.

In most cases the treatment for meningococcal meningitis is with antibiotics, where the primary aim is to achieve a rapid bactericidal effect in the CSF<sup>1</sup>. This treatment is suggested prior to positive identification of cultures of the bacteria obtained from the CSF as any delay is potentially life-threatening if the bacteria have indeed invaded the CSF<sup>4</sup>.

### 1.3 Growth of *N. meningitidis*

Bacteria require carbon and energy sources in order to grow, and these are often sourced from sugars present in the environment. *N. meningitidis* can only use the sugars glucose and maltose as carbon sources<sup>15,16</sup>, however they can use peptides as carbon sources. The bacteria are usually grown on Müller-Hinton broth and Columbia agar which are peptide-based formulations.

### 1.4 Organisation of the Respiratory Chain of *N. meningitidis*

*N. meningitidis* is classified as an aerobe and as such has an oxidase pathway for reducing oxygen (O<sub>2</sub>), but given that the environment in the nasopharynx is poor in oxygen, the bacteria must also be capable of respiring in a microaerobic



Figure 1.1: **Complete denitrification.** The process of reducing nitrite to nitrogen gas. In *N. meningitidis* the first and final steps highlighted in blue do not occur.

environment. This is evidenced by the fact that bacterial isolates from the nasopharynx routinely contain both strict aerobes and strict anaerobes<sup>17</sup>. Genomic analysis of 2 strains of *N. meningitidis* shows that there are 3 terminal oxidases; 1 of each for reducing oxygen, nitrite ( $\text{NO}_2^-$ ) and nitric oxide ( $\text{NO}$ )<sup>18</sup>. This analysis may be expanded as there are now many more genomes published. Experiments showed that under oxygen limiting conditions, *N. meningitidis* was capable of growth when nitrite was present in the media (Müller-Hinton Broth), and that nitrate ( $\text{NO}_3^-$ ), the probable source for nitrite, had no effect on growth<sup>18</sup>. Additionally the bacteria require carbon dioxide, as shown by Tuttle and Scherp<sup>19</sup> and have 2 enzymes which catalyse the reduction of  $\text{CO}_2$ <sup>4</sup>.

*In vivo*, nitrite is obtained as a product of digesting nitrate in food. There are a number of facultative nitrate-reducing bacteria present in the mouth and pharynx responsible for this<sup>17</sup> which additionally have a proposed benefit of protecting the host against periodontal and cariogenic bacteria<sup>20</sup>. Nitrite is also created by oxidation of nitric oxide, which is produced as a host signalling molecule and as a toxin as part of the host immune response<sup>17,20</sup>.

The respiratory pathway for reducing nitrite in *N. meningitidis* involves two steps; nitrite is reduced to nitric oxide, which is then further reduced to nitrous oxide. This represents incomplete reduction, as a further reduction step is possible (shown in Figure 1.1), reducing nitrous oxide to dinitrogen gas<sup>17,21</sup>.

Reduction of oxygen is favourable over nitrite reduction due to the redox potential differences. The redox potential of  $\text{O}_2/\text{H}_2\text{O}$  is +820 mV,  $\text{NO}_2^-/\text{NO}$  is +348 mV, thus  $\text{O}_2$  has a higher tendency to acquire electrons resulting in an electrochemically favourable reaction<sup>22</sup>. The electron flow towards the oxidase is also preferred physiologically as it liberates more energy by virtue of the translocation of more protons than the reduction of nitrite. The translocated protons

Reduction		Enzyme
$\text{NO}_2^-$	$\rightarrow$ NO	AniA
NO	$\rightarrow$ $\text{N}_2\text{O}$	NorB
$\text{O}_2$	$\rightarrow$ $\text{H}_2\text{O}$	<i>cbb<sub>3</sub></i>

Table 1.1: The reductions catalysed by the respiratory enzymes in *N. meningitidis*

are ultimately used in the synthesis of ATP molecules for energy. This results in reduction of oxygen in preference to nitrite when both are present (in most cases).

Reduction of oxygen in *N. meningitidis* is carried out by the oxygen reductase cytochrome *cbb<sub>3</sub>* oxidase, a membrane-bound heme-copper oxidase<sup>23</sup>. *cbb<sub>3</sub>* is capable of binding oxygen and nitric oxide, which means that during nitrite reduction (denitrification), the oxidase can be competitively inhibited (chemically) by the intermediate product of denitrification. *cbb<sub>3</sub>* can be permanently damaged at high concentrations of NO and  $\text{O}_2$ , as they can both bind at the *cbb<sub>3</sub>* active site and react together to form peroxynitrite<sup>24-26</sup>.

Nitrite is reduced by the nitrite reductase AniA, which is a copper containing reductase. This reduction does not involve translocation of protons, and thus does not produce any usable energy. Nitrite is reduced to nitric oxide which can then be further reduced by a nitric oxide reductase NorB. Since *N. meningitidis* is capable of reducing nitric oxide, a host toxin, directly, this may help it defend itself against part of the host immune response<sup>17,27</sup> as has been shown in tissue culture by Anjum et al.<sup>26</sup>.

The reduction processes carried out by these enzymes are shown in the table in Table 1.1.

The major source for electrons in both respiratory pathways is NADH, although electrons can also be obtained from pyruvate and lactate amongst others. These reduced substrates lead to reduction of ubiquinone to ubiquinol in the ubiquinone pool that exists within the bacteria. Ubiquinol is oxidised either by the cytochrome *bc<sub>1</sub>* complex or directly by the NorB enzyme whilst reducing NO to  $\text{N}_2\text{O}$ . Cytochrome *bc<sub>1</sub>* is oxidised by a number of intermediate cytochromes



Figure 1.2: **Layout of the components of the respiratory system in *Neisseria meningitidis*.** Oxygen reducing components are shown in green, nitrogen reducing components in red. Components transporting electrons are coloured light blue, and their transport is indicated by dashed arrows. Respiratory substrates are shown in dark blue, with corresponding arrows linking them to their reducing enzymes. Components which produce membrane potential are also indicated.

which act to transport electrons to the terminal oxidases; AniA and *cbb*<sub>3</sub>. The *c*<sub>5</sub> cytochrome transports electrons from the *bc*<sub>1</sub> complex to AniA, and two cytochromes, *c*<sub>2/x</sub> and *c*<sub>4</sub>, transport electrons to *cbb*<sub>3</sub>. It is not understood why *cbb*<sub>3</sub> has 2 alternate cytochromes, and there is evidence to suggest that it can also be supplied, in a limited capacity, by the *c*<sub>5</sub> cytochrome as well<sup>28</sup>. The electron transport chain is shown graphically in Figure 1.2.

In addition to the difference in favourability between the two respiratory pathways, there is also a great deal of regulation, both at the enzymatic and transcriptional level. Chemical inhibition also plays a part in regulation as briefly mentioned previously. Expression of AniA is regulated by two processes, the reduction of oxygen and the presence of nitrite. The presence of oxygen down-regulates the expression of an activator of AniA expression. This activator is FNR (fumarate and nitrate reduction regulator), and the presence of oxygen effectively means that AniA expression is repressed by the reduced expression of FNR. In *N.*

*meningitidis*, FNR appears to work slightly differently than in facultative anaerobes such as *E. coli*, in that FNR is still expressed at quite high concentrations of oxygen, and is itself down-regulated by a separate co-factor<sup>29</sup>.

The presence of nitrite triggers the two component NarP/NarQ system which activates expression of AniA in response to increasing levels of nitrite<sup>17</sup>. The activity of AniA is also controlled by the competition for electrons by the other reductase enzymes in the respiratory chain. Both NorB and *cbb<sub>3</sub>* have a higher affinity for electrons than AniA, and as a result the presence of these enzymes (when active) has an inhibitory effect on AniA. The regulation of AniA is further complicated by the production of nitric oxide, and the presence of a protein, NsrR.

Nitric oxide has a direct inhibitory effect on the expression of AniA, as does the NsrR protein. Nitric oxide also inhibits the NsrR protein, leading to a de-repression of AniA<sup>27</sup>. In the absence of nitric oxide, AniA is almost fully repressed by active NsrR. As NO concentrations increase, NsrR is inactivated allowing full activation of AniA. Once NO reaches a sufficiently high level it will begin to inhibit AniA<sup>17,29</sup>.

NorB is less tightly regulated by respiratory components, as it is only acted upon by NsrR, however it is regulated by FNR and NrsR outside the respiratory chain<sup>30</sup>. This regulation by NsrR works in a similar way to how NsrR acts upon AniA. When there is no nitric oxide present, the NsrR acts to inhibit NorB since there is no substrate for it to reduce. In the presence of nitric oxide, NsrR is inhibited, leading to the activation of NorB which is now able to reduce NO to N<sub>2</sub>O. In this case nitric oxide is acting as a de-repressor of NorB.

This complicated set of regulatory relationships between the different components of the respiratory pathways is shown in Figure 1.3.





Figure 1.3: **Regulation of respiratory components in *Neisseria meningitidis*.** Enzymes and enzymatic reactions are shown in red. A. describes the regulation caused by competition for electrons between the respiratory enzymes. B. shows the genetic regulation, which also involves a number of additional components in dark blue. C. shows chemical inhibition of the respiratory components.

## 1.5 Respiratory Enzymes in *N. meningitidis*

### 1.5.1 Cytochrome *cbb*<sub>3</sub> oxidase

Cytochrome *cbb*<sub>3</sub> oxidase is a Haem Copper Oxidase (HCO) enzyme found commonly in proteobacteria. They have been characterised in at least *Pseudomonas denitrificans*, *Rhodobacter sphaeroides*, *Rhodobacter capsulatus* and *Bradyrhizobium japonicum*<sup>31</sup>. HCOs catalyse the reduction of Oxygen molecules to water whilst translocating protons across the inner membrane, from the cytoplasm to the periplasm, producing an electrochemical gradient.

HCOs can be separated into two categories by their electron donor type. Cytochrome *c* oxidases accept electrons from *c*-type cytochromes, and quinol oxidases accept electrons from ubiquinol. The major difference between these two categories is a missing Cu<sub>A</sub> site in quinol oxidases<sup>32</sup>. HCOs can be further broken down to 3 type, the *aa*<sub>3</sub>-type cytochrome *c* oxidase, the *bo*<sub>3</sub>-type quinol oxidase and the *cbb*<sub>3</sub>-type cytochrome *c* oxidase<sup>33</sup>. Alternatively 5 different HCO subclasses may be classified, the *aa*<sub>3</sub>, *caa*<sub>3</sub> and *cbb*<sub>3</sub>-type cytochrome *c* oxidases, and the *bo*<sub>3</sub> and *aa*<sub>3</sub>-type quinol oxidases<sup>34</sup>. All of these different types of cytochrome *c* oxidases are found in bacteria, whereas those in mitochondria are limited to *aa*<sub>3</sub>-type cytochrome *c* oxidases<sup>35</sup>.

HCOs are themselves “defined by the primary sequence of their catalytic subunit, which is composed of twelve transmembrane helices with six invariant his-

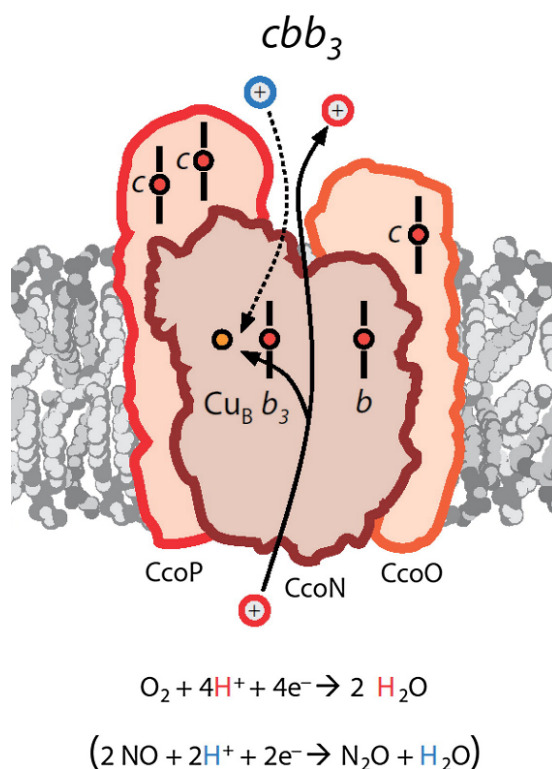


Figure 1.4: **The *cbb<sub>3</sub>* oxidase.** This diagram shows the proton input pathway for Oxygen reduction shown in red, and the putative pathway for Nitric Oxide reduction in blue. Also shown are the 3 subunits and their associated heme centres. Adapted from Huang et al.<sup>36</sup>.

tidines ligating three cofactors; a high spin heme (one His ligand) and a copper (3 His ligands) in the catalytic site and an additional low-spin heme (two His ligands)”<sup>36</sup>. Sequence alignment has also indicated that bacterial NO-reductase (NOR) might also be a divergent member of the HCO family. A schematic diagram of the *cbb<sub>3</sub>* oxidase is shown in Figure 1.4. *cbb<sub>3</sub>* is composed of three main subunits with CcoN being the catalytic subunit, which is related to subunit I of *aa<sub>3</sub>* oxidases and NorB. This latter relation to NorB explains why *cbb<sub>3</sub>* has some Nitric Oxide reduction activity (and conversely why NorB has some Oxygen reduction activity)<sup>36</sup>. CcoN contains the catalytic site – the high-spin heme *b<sub>3</sub>*-Cu<sub>B</sub> – and a low spin heme *b*. CcoO is anchored in the inner membrane and contains just one *c-type* heme. CcoP contains two *c-type* hemes and is anchored to the inner membrane. CcoQ, the fourth subunit is small, and helps to stabilise the complex<sup>36</sup>.

The mechanism of reduction of  $O_2$  by *cbb*<sub>3</sub> oxidases is not fully understood, as the reduction intermediates currently remain unknown<sup>36</sup>. The cytochrome *cbb*<sub>3</sub> oxidases have very low  $K_m$  values, allowing them to operate even under oxygen limiting conditions. *cbb*<sub>3</sub> from *Bradyrhizobium japonicum* has a  $K_m$  of 7 nM, much lower than that of the mitochondrial *aa*<sub>3</sub> oxidase<sup>37</sup>. This high affinity for oxygen suggests that *N. meningitidis* may have become adapted to surviving in the human host in areas of low oxygen concentration. Since this type of oxidase is also found in other human pathogens it is likely that it is used to allow those pathogens to survive in hypoxic environments in the human host<sup>38</sup>.

The catalytic reaction for the *cbb*<sub>3</sub> oxidase is:



### 1.5.2 NorB Nitric Oxide Reductase

Nitric Oxide Reductase is also a Haem Copper Oxidase enzyme which is found in bacteria as an integral membrane protein. There are three types of NOR, the cytochrome *bc* type complex (cNOR), the cytochrome *b* type complex lacking the cytochrome *c* component (qNOR) and a qNOR-type reductase that also includes  $Cu_A$  (qCu<sub>A</sub>NOR). cNOR-type reductases receive electrons from soluble redox protein donors, whereas qNOR-type reductases receive electrons from quinol<sup>39</sup>.

The NOR in *N. meningitidis* is a qNOR-type reductase, and is encoded by the *norB* gene (NMB1622). It catalyses the reduction of Nitric Oxide to Nitrous Oxide receiving electrons directly from the quinone pool. Under microaerobic conditions this enzyme is important as during denitrification to support growth, Nitric Oxide accumulates as a result of reduction of Nitrite. The build up of Nitric Oxide inhibits aerobic respiration as it binds competitively to the *cbb*<sub>3</sub> oxidase. NorB protects the bacteria from the toxicity extracellular NO which is produced by host tissues and macrophages, which produce NO in quantity during infection<sup>27</sup>.

The nitric oxide reductase in *Neisseria gonorrhoeae* is predicted to be an 84.3

kDa protein with significant sequence identity to *Ralstonia eutropha* and consists only of the NorB subunit<sup>39</sup>. The NorB protein is highly conserved across all *Neisseria* species as evidenced by sequence analysis<sup>40</sup>.

The catalytic reaction for NorB is:



### 1.5.3 AniA Nitrite Reductase

AniA nitrite reductase is an anaerobically induced, outer membrane associated protein which uses nitrite as an electron acceptor<sup>41</sup>. It is a copper-containing protein found in many denitrifying proteobacteria.

Nitrite reductases catalyse the reduction of nitrite to nitric oxide with no associated proton translocation. There are two types of nitrite reductase, those that have haem centres, and those which have copper centres. AniA in *N. meningitidis* is a copper-containing and accepts electrons from *c*-type cytochromes (*c*<sub>5</sub>).

In *N. meningitidis* this enzyme is important during oxygen limiting conditions as it allows microaerobic respiration which can supplement growth by denitrification<sup>17</sup>.

Interestingly, according to its genome sequence *N. meningitidis* strain 053442 appears to lack the *aniA* gene in its entirety, suggesting that this strain would be unable to perform denitrification and respire anaerobically<sup>40</sup>. 32% of *N. meningitidis* strains sequenced by Barth et al.<sup>40</sup> contain non-functional copies of *aniA* with frameshift mutations. These strains do still possess the *norB* gene for reducing Nitric Oxide however allowing them to prevent its toxic effects. It has been suggested by some that this may actually be evidence that *Neisseria meningitidis* is in the process of evolving away from denitrification to being a Nitric Oxide tolerant aerobe<sup>42</sup>.

The catalytic reaction for AniA is:



## 1.6 Respiratory Electron Transporters in *N. meningitidis*

### 1.6.1 NADH Dehydrogenase

NADH (Reduced Nicotinamide Adenine Dinucleotide) Dehydrogenase is an inner membrane bound enzyme that catalyses the transfer of electrons from NADH to the quinone pool in many bacteria. There are three types of NADH dehydrogenase enzymes found in bacteria, NDH-1, NDH-2 and  $\text{Na}^+$ -NDH. NDH-1 is related to Complex I of the mitochondrial respiratory chain and translocated protons across the inner-membrane whilst reducing the quinone pool<sup>43–45</sup>. NDH-2 does not have any proton pump activity, nor does it have any Fe-S clusters<sup>46</sup>.  $\text{Na}^+$ -NDH translocates  $\text{Na}^+$  ions across the membrane<sup>47</sup>. The NADH dehydrogenase of *N. meningitidis* is of the NDH-1 type<sup>22</sup>.

Mitochondrial complex I catalyses the oxidation of NADH and the reduction of ubiquinone whilst translocating 4 protons across the membrane. It does so using the following reaction scheme:



### 1.6.2 Cytochrome $bc_1$ Complex

The cytochrome  $bc_1$  complex oxidises quinols and reduces metalloprotein electron transporters (usually c-type cytochromes). It is an important part of bacterial respiratory chains, and is also analogous to the mitochondrial complex III<sup>48</sup>. Whilst catalysing the reduction of ubiquinol and the oxidation of c-type cytochromes, the  $bc_1$  complex also translocates protons across the inner membrane from the cytoplasm to the periplasm producing an electrochemical gradient. The  $bc_1$  complex is found in both Gram negative and Gram positive bacteria, however *E. coli* has no  $bc_1$  complex. The homolog the  $b_6f$  complex is also used for electron transfer during photosynthesis in higher plants and phototrophic bacteria<sup>49</sup>.

In bacteria the  $bc_1$  complex is formed of one cyt  $b$  subunit which contains two

*b*-type hemes, one cyt  $c_1$  subunit which contains a single *c*-type heme and an Rieske iron-sulfur protein. These subunits form the two catalytic sites of the  $bc_1$  complex. The reduction of ubiquinol appears to occur in a concerted manner at 1 of these sites,  $Q_o$ <sup>49</sup>. Electrons from the quinol are shared between two reaction chains, 1 which transfers electrons to the high-potential iron-sulfur protein and  $c_1$ , and another which transfers electrons to the low-potential cytochrome *b*. The other catalytic site  $Q_i$  uses the two electrons from the high and low potential chains to reduce quinone, or other metalloprotein electron transporters<sup>50,51</sup>. This modified Q-cycle is shown in Figure 1.5.

The reaction scheme for the  $bc_1$  complex is:



### 1.6.3 Cytochromes $c_4$ , $c_x$ and $c_5$

Cytochromes  $c_4$ ,  $c_x$  and  $c_5$  are soluble *c*-type cytochromes. These are small heme proteins that are found in the periplasm and are loosely associated with the inner membrane. Along with their presence in proteobacteria, the *c*-type cytochromes also form part of the mitochondrial respiratory apparatus in the form of cytochrome *c*. Bacterial *c*-type cytochromes perform a very similar function to mitochondrial cytochrome *c* in that they transport electrons from the  $bc_1$  complex to the terminal reductases. Cytochromes  $c$ -552,  $c$ -553 &  $c$ -554 from algal chloroplasts and cyanobacteria,  $c_2$  from purple photosynthetic bacteria and  $c_4$  and  $c_5$  from *Azotobacter vinelandii* along with many others all have sequence and structural homology with mitochondrial cytochrome  $c$ <sup>53</sup>. The mitochondrial and bacterial soluble cytochromes all fall within Ambler's Class I of *c*-type cytochromes<sup>54</sup>. Class I *c*-type cytochromes have their heme-attachment site towards the N-terminus, and the sixth ligand is provided by a methionine residue 40 residues further down the chain towards the C-terminus<sup>54</sup>[Re-write this sentence, it is almost plagiarism!]. Cytochrome  $c_4$  is a diheme cytochrome and is the electron donor to  $cbb_3$  transfer-

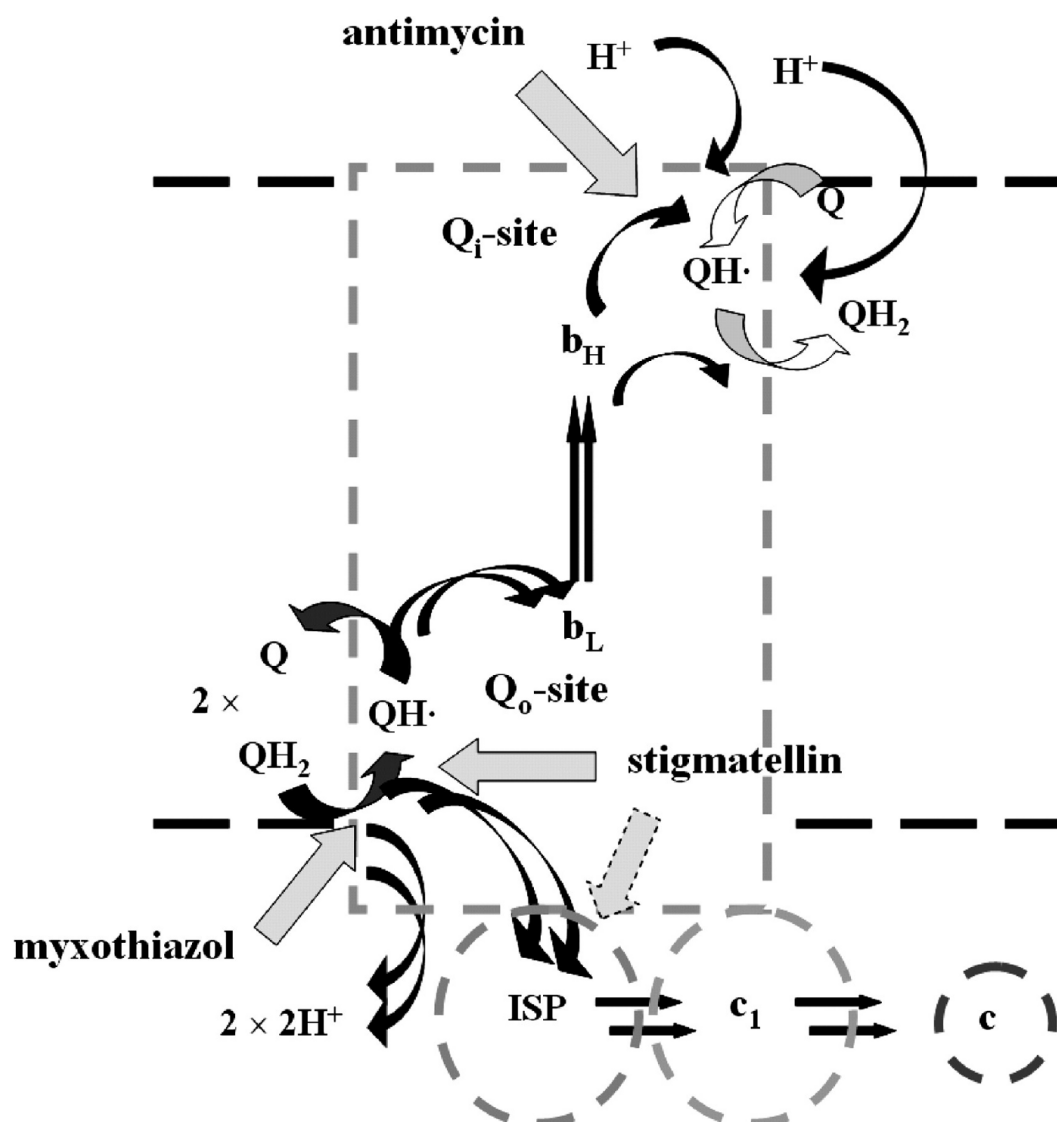


Figure 1.5: **The modified Q-cycle used by the bacterial  $bc_1$  complex.** The cyt  $b$  subunit is represented by the *dashed gray* outline, and contains the  $Q_0$ - and  $Q_i$ -sites, connected by hemes  $b_L$  and  $b_H$ . The ISP and cyt  $c_1$  catalytic domains and cyt  $c$  are represented by *dashed darker gray* circles. Electron transfer steps are shown by *dark narrow arrows*, proton release and uptake by *lighter arrows*, binding and release of quinone species by *broad curved arrows* (dark gray for  $Q_0$ -site, light gray for  $Q_i$ -site). Sites of inhibition are indicated by *block arrows* showing sites at which the bound inhibitor displaces quinone species. The *dashed inhibitor arrow* indicates that the reaction of ISPH with cyt  $c_1$  is blocked by the interaction of ISPH with stigmatellin at the  $Q_0$ -site. Adapted from Crofts et al.<sup>52</sup>.



Figure 1.6: Structure of the ubiquinone molecule.

ring electrons from the  $bc_1$  complex in *N. meningitidis*<sup>22,28,55</sup>.

Cytochrome  $c_x$  is a monoheme cytochrome which is also able to transfer electrons from the  $bc_1$  complex to  $cbb_3$ <sup>22,28</sup>.

Cytochrome  $c_5$  is a diheme cytochrome which appears to be membrane associated. It transfers electrons from the  $bc_1$  complex to AniA during Nitrite reduction<sup>22,28</sup>.

#### 1.6.4 Quinone Pool

The quinone source in *N. meningitidis* is predicted to be ubiquinone<sup>22</sup>. Ubiquinone, also known as Coenzyme Q<sub>10</sub> is found in most eukaryotes. It is a vitamin-like lipid soluble molecule with a long tail made of 10 isoprenyl subunits. This is shown in Figure 1.6.

In its oxidised form it is known as ubiquinone, whereas when reduced it is called ubiquinol. In the *N. meningitidis* respiratory chain, ubiquinone is reduced to ubiquinol by the acceptance of 2 electrons from NADH (amongst others). Ubiquinol then donates electrons either directly to the terminal reductase NorB, or to the  $bc_1$  complex.



## 1.7 Respiration Regulatory Proteins in *N. meningitidis*

### 1.7.1 NsrR - Nitrite Sensing Repressor Protein

“NsrR is an NO-sensing Rrf2-type transcriptional repressor”<sup>40</sup>. In *N. meningitidis* (and *N. gonorrhoeae*) it negatively regulates *aniA* and *norB*, and derepression is caused by NO<sup>27,29,30</sup>. Rrf2 proteins have two DNA-binding helix-helix domains<sup>29</sup>, with a putative iron-sulfur cluster inbetween. The binding of the iron-sulfur cluster, which is expected to be by NO in NsrR, would perturb the structure of the repressor protein and prevent DNA binding<sup>29</sup>.

*norB* is expressed in a somewhat constitutive manner, in that with no repression *norB* is still expressed to some extent<sup>56</sup>. NsrR represses this expression until NO is present, at which point *norB* can be expressed and the NorB enzyme can start removing the NO that is present.

*aniA* is positively regulated by FNR, but this seems to be quite insensitive to oxygen in *N. meningitidis*, thus *aniA* would be expressed even at 60 to 80% air saturation with oxygen<sup>29</sup>. *aniA* therefore needs to be corepressed in order to prevent it being expressed excessively in aerobic conditions.

### 1.7.2 FNR - Fumarate and Nitrate Reductase Regulator

Fumarate Nitrate Reductase is a transcriptional activator which binds to a 4Fe-4S cluster under anaerobic conditions. When oxygen concentrations are low, FNR causes increased expression of proteins that are necessary for anaerobic respiration. “The presence of the 4Fe-4S cluster is correlated with protein dimerization, which enables it to bind promoter DNA”<sup>57</sup>. Four cysteine residues are believed to be ligated to the iron-sulfur cluster and these are required for FNR function. The oxygen sensitivity of FNR is achieved by the iron-sulfur cluster breaking down into 2Fe-2S via 3Fe-4S which is unable to bind DNA. In *N. meningitidis*, *aniA* expression is directly linked to the presence of FNR<sup>17</sup>. When no NsrR is present, *aniA* expression continues even up to 80% oxygen saturation suggesting

that FNR is actually quite insensitive to oxygen, an unusual response compared to FNR from *E. coli*. FNR also becomes less sensitive to oxygen when it is bound to its cognate DNA<sup>57</sup>.

### 1.7.3 NarQ/NarP - Nitrite Response Sensor/Regulator

NarP and NarQ are a two component signal transduction pathway that regulate expression of *aniA* in *Neisseria*. NarQ is the sensor protein located in the inner membrane, while the regulator protein, NarP is found in the cytoplasm. Being a two component system, the sensor protein phosphorylates the regulator allowing it to bind the target DNA (which may consist of multiple sequences) to activate expression of genes.

In *N. gonorrhoeae*, NarP was shown to enhance the expression of *aniA* in response to the presence of nitrite, as a mutant lacking *narP* was significantly slower at growing under denitrifying conditions<sup>58</sup>.

In *N. meningitidis* expression of *aniA* is increased greatly in conditions of high nitrite concentration<sup>17</sup>. This effect is much more pronounced than simply being in oxygen limiting conditions. FNR appears to be required for *aniA* expression even when NarP/NarQ are present<sup>17</sup>. This suggests that the organism is intentionally preventing expression of nitrite reducing components until there is both a high concentration of nitrite *and* a very low concentration of oxygen. This is plausible as even under oxygen limiting conditions oxygen reduction is still favoured over nitrite reduction.

## 1.8 Organisation of Respiratory Chains in Other Bacteria

The respiratory chain of *N. meningitidis* is shown in a simplified form in Figure 1.7. The components are coloured consistently throughout this section to allow easy comparison between the respiratory chains being discussed. As discussed previously, the respiratory chain of *N. meningitidis* contains an initial electron donor, in this case NADH dehydrogenase. In fact there are a number of other



Figure 1.7: **Branched electron transport chains of *N. meningitidis*.** Blue denotes initial electron donor, red denotes quinone pool, purple denotes cytochrome electron transporters and green denotes terminal reductases. UQ = ubiquinone.

electron donors, but they are not discussed here as NADH provides most of the electrons to the respiratory chain. There is also a quinone pool, consisting of ubiquinone/ubiquinol, intermediate *c*-type cytochromes and terminal reductases.

### 1.8.1 The Respiratory Chain of *Paracoccus denitrificans*

The respiratory chain of *P. denitrificans* is shown in Figure 1.8. It is quite similar to that of *N. meningitidis* with the exception of having a larger number of terminal reductases, and the ability to perform complete denitrification. The chain possesses an initial electron donor, a quinone pool, intermediate cytochrome electron transporters and terminal reductases.

The *bc*<sub>1</sub> complex of *N. meningitidis* is present as an analogue (Ubiquinol-cyt *c* oxidoreductase), and the chain includes 2 further downstream *c*-type cytochromes. *P. denitrificans* has 3 terminal oxygen reductases, *ba*<sub>3</sub>, which oxidises the quinone pool directly, and *cbb*<sub>3</sub> and *aa*<sub>3</sub> which oxidise the *c*-type cytochromes. All three oxygen reductases are HCOs. The branching of the aerobic electron transport

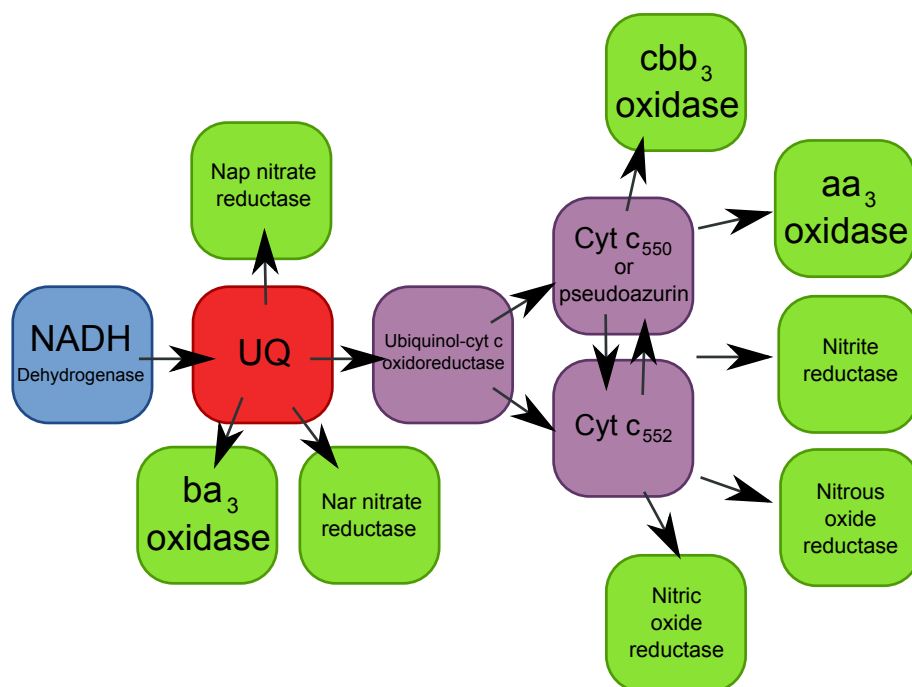


Figure 1.8: **Branched electron transport chains of *Paracoccus* species.** Blue denotes initial electron donor, red denotes quinone pool, purple denotes cytochrome electron transporters and green denotes terminal reductases. UQ = ubiquinone. Electron transfer between cytochromes  $c_{552}$  and  $c_{550}$  has not been demonstrated experimentally but is possible, given the redox potential of the proteins. Adapted from Baker et al.<sup>59</sup>.

chain is quite common among bacteria, but the reason for this is not currently fully understood.

The nitro-reductases found in *P. denitrificans* are capable of complete denitrification as described in Figure 1.1. The nitrate reductases directly oxidise the quinone pool, whereas the nitrite and nitric oxide and nitrous oxide reductases oxidise the *c*-type cytochromes instead.

As with *N. meningitidis* there are a number of potential initial electron donors, but only NADH is shown for simplicity of comparison.

### 1.8.2 The Respiratory Chain of *Escherichia coli*

The respiratory chain of *E. coli* is shown in Figure 1.9. It can be seen to be quite distinct from other bacteria, and indeed from the mitochondrial respiratory chain. The most obvious difference between *E. coli* and many other bacteria is the lack of *c*-type cytochromes. The terminal reductases are able to be reduced directly



Figure 1.9: **Branched electron transport chains of *E. coli*.** Blue denotes initial electron donor, red denotes quinone pool and green denotes terminal reductases. UQ = ubiquinone. Under anaerobic conditions, ubiquinone is replaced by menaquinone. Adapted from Nicholls and Ferguson<sup>60</sup>.

by the quinone pool. Additionally, under anaerobic conditions, the quinone pool changes from being ubiquinone/ubiquinol to menaquinone/ubiquinol.

*E. coli* also has a number of different terminal reductases in the form of cyt *bo*<sub>3</sub> and cyt *bd*. Cyt *bo*<sub>3</sub> is an HCO and is structurally very similar to cyt *aa*<sub>3</sub>. Cyt *bd* shows no sequence similarity with the HCO superfamily and has no Cu<sub>B</sub> site. Cyt *bd* has a much higher affinity for oxygen than cyt *bo*<sub>3</sub> so is synthesised at low oxygen concentration.

*E. coli* is also capable of partial denitrification and possesses enzymes to reduce nitrate and nitrite, which are also under the regulatory control of FNR. The reduction of nitrite differs from *N. meningitidis* and *P. denitrificans* as NO<sub>2</sub><sup>-</sup> is not reduced to NO, but to NH<sub>4</sub><sup>+</sup> instead.

As with *N. meningitidis* and *P. denitrificans* there are a number of potential initial electron donors, but only NADH is shown for simplicity of comparison.

## 1.9 Systems Biology

Systems biology is the process of “studying biological systems in their whole [...], reinforced by high throughput [...] molecular tests and considerable sophistication in computational modelling”<sup>61</sup>. Systems biology “combines approaches and methods from systems engineering, computational biology, statistics, genomics, molecular biology, biophysics and other fields”<sup>62</sup>.

The aim of Systems biology is to take our detailed understanding of organisms beyond the molecular and cellular level. These are the levels to which the disciplines of molecular and biology and biochemistry (among others) are more suited. It aims to take our understanding to the level of the entire “complex system”. Which is to say we gain understanding into the way the organism behaves as a whole, rather than just having knowledge of the individual parts.

The level of complexity in biological systems is far greater than the popular notion of what defines a complex system, however. Biological systems consist of multiple different individual elements each performing specific tasks interacting with each other to create ‘coherent’ behaviour. This is very different from popular complex systems which are collections of simple, identical components interacting to produce ‘complex’ behaviour<sup>63</sup>.

Gaining understanding such a complex system is difficult, and Kitano suggests that it requires insight into the following properties<sup>64</sup>:

1. **Structure of the system.** This includes the way the system interactions are “laid out” both at a component level and an organismal level.
2. **The dynamics of the system.** This involves understanding how the organism behaves under any given conditions over a particular time period. This may include understanding how the metabolic processes change under these conditions etc.
3. **How the system is controlled.** The control mechanisms can be tailored to suit the desired function or to minimised the chance of malfunction.



Figure 1.10: **Systems biology cycle.** Interactions between experimental analysis and theoretical approaches, and the main tasks for theory at the interfaces. Doyle and Stelling<sup>62</sup>

4. **How the system is designed.** “Trial and error” experimentation can be done away with, as the system can be designed based on defined properties, backed up by models and simulations.

The level of integration between systems biology approaches and experimentation can be seen in Figure 1.10. This shows the iterative cycles that are necessary to gain understanding in both areas. The experimentation provides data to refine and develop the system model, and data from that model can go on to improve the design of the experiment.

Systems biology extends further into a computational discipline when you consider that if you can create a model of a system, you can potentially run a simulation of the system using the model. Simulations can be developed for multiple stages of the process, from molecular to organismal. Simulations of interactions based on gene regulatory network models are being studied<sup>65</sup>, as are complete plant development models<sup>66–68</sup>.

Figure 1.11 shows one of the limitations of the current technology “powering”



Figure 1.11: **System complexity.** Diagram showing how system complexity varies across organisms, and how the complexity of the models we can produce is currently the inverse of systems complexity. Kahlem and Birney<sup>61</sup>

systems biology. As organisms get more complex, the models we can produce get less complex and less quantitative<sup>61</sup>. This concomitant lack of data in models of complex organisms decreases the likelihood of being able to produce a simulation of the model. We might be able to simulate *aspects* of a complex organism, such as the human heart<sup>69</sup> but we are still a long way from being able to simulate the entire human body.

For simpler systems, like yeast, or *E. coli* an enormous amount of data already exists about individual gene regulation, protein interactions etc. and it is possible to build sophisticated models of the entire gene regulatory network and more<sup>70,71</sup>.

A systems biology approach to understanding the mechanism of respiration in *Neisseria meningitidis* is necessary as there are a number of components in the system which are inherently unmeasurable.



## 1.10 Modelling

### 1.10.1 Modelling Respiratory Systems

A limited amount of modelling has been carried out on bacterial respiratory chains, these focused on the denitrification pathway and treated the pathway as a simple electrical circuit<sup>72</sup>. An alternative approach involved modelling respiration using “P systems” which are probabilistic models of events. This assigned a probability of each reaction happening, dependant on the state of the system and then iterated through a given set of steps evaluating probabilities and altering values based on the outcome<sup>73</sup>. This approach to modelling was limited in that it was only predicting the quantities of 1 component in each of 2 “compartments”; oxygen in the cell membrane and carbon dioxide in the thylakoid membrane (the model was developed using cyanobacteria).

Some modelling of parts of the respiratory chain in *E. coli* have also been modelled. Peercy et al.<sup>71</sup> created a kinetic model of how cytochrome production is regulated by oxygen using differential equations. They created a set of differential equations to describe the relevant reactions and then populated the model using parameters gathered from the literature.

Since when modelling respiration in a cell, the most important factor is the change in concentration of components over time without any particular spatial constraints, ordinary differential equations (ODEs) are an appropriate technique. In these systems the model does not change with regard to the spatial arrangement of any of the components. If the system requires changes in time *and* space, then partial differential equations (PDEs) would be necessary (and more complicated)<sup>74</sup>.

Ordinary differential equations only depend on one variable; the time ( $t$ ). In this case, the change in concentration over time for each component can be modelled as a single differential equation. For multiple components this leads to multiple differential equations with some that rely on the result of another (if the rate

of one reaction is directly related to the concentration of another component). These ODEs must then be solved in parallel at a suitable time-scale.

Complications arise when using differential equations if the processes are considered to be stochastic, as a differential equation model assumes that every component can have a continuous value, which is not the case as molecules are discrete. However if the system being modelled is sufficiently large, this effect can be ignored. If the reaction component size is small ( $< 100$ s of molecules) stochastic simulation algorithms have to be used as described by Gillespie<sup>75</sup>. This method requires far more computation than solving ODEs, as the model will spend most of its time calculating values for reactions involving large molecules even though this is not necessary as the reaction is not stochastic. Additionally, the time interval used between reaction steps is usually very small, meaning the simulation progresses slowly<sup>74</sup>.

#### 1.10.2 Modelling Tools

A number of software packages exist that are capable of this type of modelling such as the Systems Biology Workbench<sup>76</sup> and COPASI<sup>77</sup>. These allow you to enter biochemical reactions in a format familiar to biologists, and have pre-defined libraries for types of reactions such as mass-action, or one with Michaelas-Menton kinetics etc. The mathematical equations are then derived automatically from the reactions and can be modified by hand if necessary. Parameters for the mathematical equations must be entered, and these will usually be derived from experimental data, or in some cases educated guesses (at least initially). Once a parameter set has been created, the modelling software can run a time-course using a relevant solver-algorithm. COPASI includes 4 solvers, LSODA (Livermore Solver for Ordinary Differential Equations)<sup>78</sup> for deterministic systems (such as ODEs), Gibson-Bruck<sup>79</sup> for stochastic systems and Runge-Kutta and LSODA for hybrid systems (where portions are not considered to be stochastic).

### 1.11 Aims

The over-arching aim of this study was to produce a working mathematical model of the respiratory system of *N. meningitidis* which has been refined and parametrised by experimental biological data. This mathematical model should be able to accurately simulate experimental datasets with known outcomes, and also be able to predict the outcome of experiments that have not been performed. This model, will also be able to provide insight into the states of various components throughout the respiratory process, such as enzymatic oxidation states, some of which are very difficult, if not impossible, to obtain in an *in vivo* study.

The layout of *N. meningitidis* respiratory chain, even though it is longer than that of the model organism *Escherichia coli* is more similar to most other bacteria. This, along with its profound medical importance make it an excellent target for the type of mathematical modelling described above.

The individual aims of the study are therefore:

1. **Construct a mathematical model of the *N. meningitidis* respiratory chain.**

This will involve the conversion of the kinetic reactions involved in respiration into mathematical equations that can be linked together, and if justified simplifying the chain.

2. **Obtaining experimental data on respiratory rates and enzyme kinetics.**

This will involve performing experiments on respiring *N. meningitidis* and recording the concentrations of respiratory substrates under different conditions.

3. **Parametrise the model using experimental data.** To do this a system will need to be developed which can iteratively fit experimental data to specific parts of the mathematical model.

# Chapter 2

## Materials and Methods

### 2.1 *Neisseria meningitidis* Strains Used in This Work

Name	Description	Source
MC58	Wild-Type Strain	McGuinness et al. <sup>80</sup>
$\Delta norB::spc^r$	Wild-Type with insertion of spectinomycin resistance cassette into <i>norB</i> gene	Heurlier et al. <sup>27</sup>
$\Delta nsrR::spc^r$	Wild-Type with insertion of spectinomycin resistance cassette into <i>nsrR</i> gene	Rock et al. <sup>29</sup>
$\Delta norB::spc^r$ - $\Delta nsrR::tet^r$	Wild-Type with insertion of spectinomycin resistance cassette into <i>norB</i> and insertion of tetracycline resistance cassette into <i>nsrR</i> genes	Heurlier et al. <sup>27</sup>
$\Delta aniA::spc^r$ - $\Delta nsrR::tet^r$	Wild-Type with insertion of spectinomycin resistance cassette into <i>aniA</i> and insertion of tetracycline resistance cassette into <i>nsrR</i> genes	Heurlier et al. <sup>27</sup>

Table 2.1: Bacterial strains and sources

## 2.2 Culturing *Neisseria meningitidis*

### 2.2.1 Growth of *Neisseria meningitidis*

*N. meningitidis* strains were grown on plates on Columbia Agar Base (CAB) with defibrinated horse blood, and in liquid culture in Müller-Hinton Broth (MHB).

Plates were prepared by adding horse blood to a final concentration of 5% to molten agar, and poured into plastic petri dishes. After streaking with *N. meningitidis* the plates were incubated at 37 °C in a 5% carbon dioxide/air mixture.

Aerobic liquid cultures were grown in 10 ml MHB with 10 mM NaHCO<sub>3</sub> in plastic sterilin tubes, and incubated at 37 °C at 200 rpm. Microaerobic cultures were suspended in 20 ml MHB, 10 mM NaHCO<sub>3</sub> in plastic sterilin tubes, incubated at 37 °C at 100 rpm.

### 2.2.2 Preparation of Antibiotic Selective Media

Liquid stock solutions of required antibiotics were either added directly to liquid culture, or, if growing on plates, to the molten agar when also adding horse blood. The final concentrations of antibiotics are given in Table 2.2.

Antibiotic	Final concentration (µg/ml)
Spectinomycin	50
Tetracycline	2.5
Chloramphenicol	50

Table 2.2: Final antibiotic concentrations

### 2.2.3 Preparation of Frozen Bacterial Stocks

Bacteria were grown in liquid culture until late log phase prior to harvesting. Liquid cultures were then centrifuged at 4000 g for 15 minutes, and the pellet was then resuspended in a 25% glycerol, 25% water and 50% MHB, all of which had been autoclaved beforehand. The bacterial stocks were then frozen at –80 °C.

#### 2.2.4 Streaking Plates for OD to CFU Ratio Calculation

Bacterial cultures were grown overnight and then transferred into aerobic liquid culture and samples taken throughout the day to obtain a range of different optical densities. The optical density was recorded at 600 nm on a Jenway 6300 Spectrophotometer (Bibby Scientific Limited, Staffordshire UK), and each sample was serially diluted to the following levels:  $10^{-5}$ ,  $10^{-6}$  and  $10^{-7}$ . 100  $\mu$ l of each of these dilutions was plated on a fresh blood agar plate and left to grow overnight. The following morning the number of colonies on each plate was counted and used to create a simple conversion factor for Optical Density to Colony Forming Units.

### 2.3 Measuring Oxygen Concentration

Oxygen concentration in respiring cultures was measured using a Clark electrode<sup>81</sup> from Rank Brothers, Cambridge, UK. This electrode has a silver anode and a platinum cathode and uses a saturated potassium chloride solution as electrolyte. The electrode is set at the bottom of a 7 ml reaction chamber separated from its contents by a thin Teflon membrane. This membrane is permeable to dissolved oxygen, which is reduced by the electrode producing a measurable electrical current. The reaction chamber is maintained at 37 °C by an attached water bath. When performing experiments, 5 ml of culture is added to the reaction chamber, which is stirred by use of a magnetic flea, and the chamber covered with a plastic stopper. The stopper has a number of holes through which the NO probe, or Hamilton syringe can be inserted. Data is collected by attaching the electrode to an external data logger (Pico ADC20, Pico Technology).

#### 2.3.1 Calibration of Oxygen Electrode

Calibration of the oxygen electrode assumes that anaerobic water will not produce any measurable current at the electrode. Oxygen saturated water contains 210  $\mu$ M Oxygen at 37 °C (ref needed). 5 ml of ultra pure water was added to

the electrode chamber, and then aerated to saturation by use of a pasteur pipette. The maximum value recorded by the data logger then corresponds to a concentration of 210  $\mu\text{M}$  Oxygen, with the relationship between mV as recorded against concentration being linear.

## 2.4 Measuring Nitric Oxide Concentration

Nitric Oxide concentration was measured using a Nitric Oxide probe (ISO-NOP, World Precision Instruments) connected to a Nitric Oxide Meter (ISO-NO mkII, World Precision Instruments). This is also a Clark type electrode, contained within a steel sleeve with a semi-permeable membrane separating the working electrode from the system being measured<sup>82–84</sup>. The NO probe is inserted through one of the holes in the plastic lid of the reaction chamber of the oxygen electrode assembly. The tip of the electrode should be immersed in the culture, with care being taken not to trap any air bubbles on the surface of the probe. The sensor is also attached to the same data logger as above. In this way both Oxygen and Nitric Oxide concentrations can be measured in parallel.

### 2.4.1 Calibration of Nitric Oxide Electrode

Calibration of the nitric oxide electrode relies on adding known quantities of Nitric Oxide to the electrode chamber. Sodium Nitrite will liberate Nitric Oxide with a 1:1 ratio when added to a solution of excess Potassium Iodide and Sulfuric acid based on the following reaction:



5 ml of 0.1M Potassium Iodide/Sulfuric Acid was added to the electrode chamber and allowed to stabilise. Then, increasing concentrations of Sodium Nitrite solution were successively added to produce a standard curve of Nitric Oxide concentration to recorded electrode mV. The volume and concentrations of Sodium Nitrite added to the electrode chamber are detailed in Table 2.3.

NaNO <sub>2</sub>		NO
Concentration ( $\mu$ M)	Volume ( $\mu$ l)	Concentration (nM)
10	50	99
100	25	591
100	50	1561

Table 2.3: Sodium Nitrite concentrations used to calibrate ISO-NOP Nitric Oxide sensor.

## 2.5 Measuring Nitrite Concentration (Griess Assay)

Nitrite concentration in liquid culture was determined using the colorimetric assay described by Nicholas and Nason<sup>85</sup>. This reaction is based on chemical diazotization which uses sulfanilamide and *N*-1-naphthylethylenediamine dihydrochloride (NED) under acidic (hydrochloric acid) conditions. Nitrite is converted to nitrous acid under acidic conditions and this then forms a diazonium salt with the sulfanilamide. The diazonium salt combines with NED and forms a pink azo dye which can be detected using absorbance spectrophotometry at a wavelength of 540 nm. Depending on the expected concentration of nitrite, different sample volumes are used in the assay. The most common sample volume used was 25  $\mu$ l which allows detection up to around 1 mM nitrite with the following reagent volumes: 875  $\mu$ l of 1% sulfanilamide in 1 M HCl and 100  $\mu$ l of 0.02% NED in 1 M HCl. When using different sample volumes, the volume of sulfanilamide was altered such that the volume of sample + sulfanilamide always equalled 900  $\mu$ l. After adding the sample to the reagents, it was left for 20 minutes for the colour to develop, then the absorbance at 540 nm was measured and compared to a standard curve.

## 2.6 Nitric Oxide Production

Solutions of Nitric Oxide were prepared using a method derived from one described by Aga and Hughes<sup>86</sup>. The apparatus setup is shown in Figure 2.1. A concentrated solution of Sulfuric acid is added from a pressure-equalizing dropping funnel to a concentrated solution of Sodium Nitrite solution in a stirred,



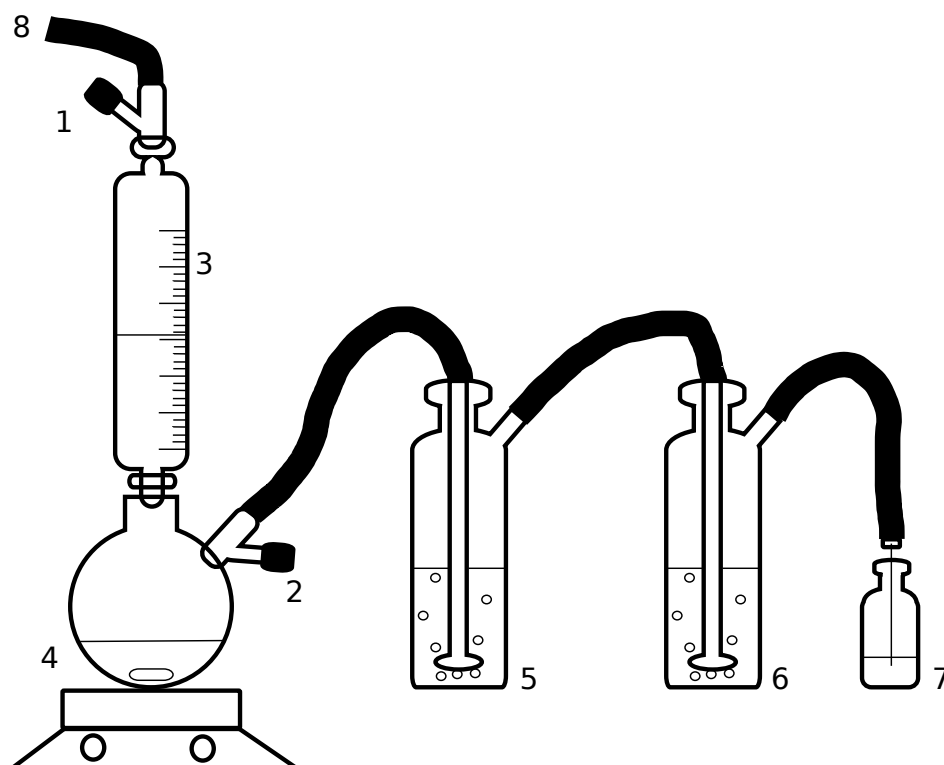


Figure 2.1: **NO making apparatus.** 1 & 2 -  $\text{N}_2$  release valves. 3 - Pressure equalizing dropping funnel, containing 50 ml 4 M  $\text{H}_2\text{SO}_4$ . 4 - Stirred, round-bottomed flask, containing 200 ml 2 M  $\text{NaNO}_2$ . 5 - Dreschel bottle with sintered bulb, containing 200 ml 1 M  $\text{NaOH}$  ( $\frac{2}{3}$  full). 6 - Dreschel bottle with sintered bulb, containing 200 ml  $\text{dH}_2\text{O}$  ( $\frac{2}{3}$  full). 7 - Small glass bottle with rubber septum and needle entry valve, containing  $\text{dH}_2\text{O}$   $\frac{2}{3}$  full. 8 - To  $\text{N}_2$  gas bottle.

round-bottomed flask. This releases  $\text{NO}$  gas which passes through a solution of Sodium Hydroxide to neutralise any Sulfuric acid present, then through distilled water to remove any Sodium Hydroxide before finally being bubbled into a collection vessel with a sealed rubber septum containing distilled water. The concentrations of the chemicals used in this preparation are shown in Table 2.4.

Chemical	Volume (ml)	Concentration (M)
$\text{NaNO}_2$	200	2
$\text{H}_2\text{SO}_4$	50	4
$\text{NaOH}$	200	1

Table 2.4: Chemicals needed for preparation of Nitric Oxide solution.

The system should be set up in a fume cupboard as shown in Figure 2.1 and sparged with  $\text{N}_2$  gas for 15 minutes (the dropping funnel will allow gas to pass

into the round bottomed flask even when the bottom valve is closed). The  $\text{H}_2\text{SO}_4$  should be sparged separately. Valve 2 should be left open at all times. After sparging close valve 1 and then add the Sulfuric acid dropwise from the dropping funnel. Brown gas will start to bubble through to the collection vessel. This apparatus should produce enough NO gas to saturate several small (10 ml) collection vessels which should have the needle removed and be sealed once saturated. Once all the Sulfuric acid has been added leave the reaction to finish which could take 1-2 hours. Before disassembly the apparatus should be sparged with  $\text{N}_2$  gas to remove residual NO gas.

The eventual concentration of NO in the solution will vary depending on the temperature, but at 25 °C in pure water the concentration will be between 1.88 and 1.96 mM<sup>86,87</sup>.

# Chapter 3

## Model - Construction and Parameters

### 3.1 Construction

The model was constructed based on existing knowledge of the respiratory chain in *Neisseria meningitidis* from the electron transport chain shown in 1.2. I made no *a priori* assumptions about separation of time-scales that would permit the use of Michaelis-Menton kinetics, as the rates of intermediate reaction steps are not known. The model was generated as a set of ordinary differential equations which describe the bulk-average concentration of substrates, products, enzymes and their activity. I have made no assumptions about the bacterial population structure and as such any stochastic effects are ignored.

#### 3.1.1 Converting Biological Reactions into Differential Equations

Where the reaction is describing a chemical process, the rate constant is given above the arrow, and the relevant enzyme shown in parentheses. Where the reaction is showing the addition of electrons (reduction), this is denoted by  $e^-$  below the arrow, the rate constant above, and the source of electrons in parentheses.

The equation that gives the change in oxygen concentration is

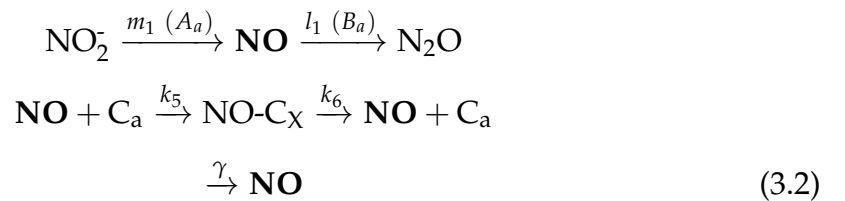
$$\frac{d[O_2]}{dt} = \beta(1 - [O_2]/K_O) - k_1[C_a][O_2]$$



where  $\beta$  is the rate of passive diffusion of  $O_2$  into the electrode chamber. This is inversely proportional to oxygen concentration in the chamber, and limited to the oxygen saturation concentration,  $K_O$ . This component of the equation is required to account for a peculiarity of the experimental set-up, whereby the rate of diffusion of oxygen into the system depends on the density of the bacterial culture, and is not insignificant.  $k_1$  is the rate of reduction of oxygen by the oxygen reductase  $cbb_3$ . This rate depends on the concentration of reduced (i.e. active)  $cbb_3$ ,  $C_a$  and the concentration of  $O_2$ .

The equation for describing NO concentration changes is more complex as NO has a number of additional interactions in comparison to  $O_2$ . NO also interacts with  $cbb_3$ , in addition to being reduced from  $NO_2^-$ , reduced to  $N_2O$  and spontaneously lost from the electrode chamber. Currently this is the equation being used to model NO concentration.

$$\frac{d[NO]}{dt} = m_1[NO_2^-][A_a] - l_1[NO][B_a] - k_5[C_a][NO] + k_6[C_X] - \gamma[NO]$$



The synthesis of NO is modelled by  $m_1$  which is the rate of  $NO_2^-$  reduction by reduced (active) AniA. This also depends on the concentration of  $NO_2^-$  and

reduced AniA ( $A_a$ ). The reduction of NO requires  $l_1$  which is the rate of reduction of NO by reduced (active) NorB. This depends on the concentration of NO and reduced NorB ( $B_a$ ). Inhibition of  $cbb_3$  by NO is modelled by the 3<sup>rd</sup> component of the equation.  $k_5$  is the rate of inhibition of  $cbb_3$  by NO.  $k_6$  is the rate of recovery of inhibited  $cbb_3$ .  $\gamma$  is the rate of spontaneous loss of NO from the electrode chamber.

The reduction of nitrite is modelled by this equation

$$\frac{d[NO_2^-]}{dt} = -m_1[NO_2^-][A_a]$$

$$NO_2^- \xrightarrow{m_1 (A_a)} NO \quad (3.3)$$

where  $m_1$  is the rate of reduction of  $NO_2^-$  by reduced (active) AniA ( $A_a$ ).

In addition to the rate of change of concentration of the respiratory substrates, the model also contains information about the state of the quinone pool, which is the upstream source of electrons into the respiratory chain. This is important because this affects the rate of reduction of the various enzymes which perform the substrate reductions. The equation for modelling the change in reduction state (activity) of the quinone pool is

$$\frac{d[Q_a]}{dt} = g([Q] - [Q_a]) - l_3[Q_a]([B] - [B_a]) - f[Q_a]([X] - [E])$$

$$\begin{aligned} & \xrightarrow[e^-]{g} Q_a \\ B_i & \xrightarrow[e^-]{l_3 (Q_a)} B_a \\ X-E & \xrightarrow[e^-]{f (Q_a)} E \end{aligned} \quad (3.4)$$

$Q_a$  is the reduced quinone, and  $Q$  the total concentration of quinones in the system.  $g$  represents the rate of flow of electrons into the quinone pool from

NADH. The rate of reduction of NorB by active quinones is given by  $l_3$ . NorB and reduced NorB are given by  $B$  and  $B_a$  respectively. As the quinones also reduce the cytochromes, this also needs to be modelled.  $f$  denotes the rate of reduction of cytochromes by the active quinones. Cytochromes and reduced cytochromes are given by  $X$  and  $E$  respectively.

Given that the concentration of active cytochromes changes, due to reduction by the quinone pool and oxidation by the downstream enzymes, and this concentration is a parameter in (3.4), it also needs to be included in the model, and this is given by the following equation

$$\frac{d[E]}{dt} = -k_3([C] - [C_a] - [C_X])[E] - m_3([A] - [A_a])[E] + f[Q_a]([X] - [E])$$



where  $k_3$  is the rate of reduction of the cytochrome c oxygen reductase ( $ccb_3$ ) by the quinone pool (via  $c_x$  &  $c_4$ ).  $C$ ,  $C_a$  and  $C_X$  represent the overall concentration of  $ccb_3$ , reduced (active)  $ccb_3$  and NO inhibited  $ccb_3$  respectively.  $m_3$  is the rate of reduction of AniA by the cytochrome pool (via  $c_5$ ). The concentration of active cytochromes increases by their reduction by the quinone pool.

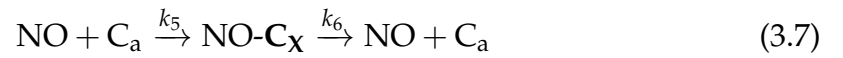
To model the changes in concentration of the individual enzymes,  $ccb_3$ , AniA and NorB, the following equations are used:

$$\frac{d[C_a]}{dt} = k_3([C] - [C_a] - [C_X])[E] - k_1[C_a][O_2] - k_5[C_a][NO]$$



This equation models the concentration of reduced (active)  $cbb_3$ , and the following equation models the concentration of  $cbb_3$  that has been inhibited by NO.

$$\frac{d[C_X]}{dt} = k_5[C_a][NO] - k_6[C_X]$$



Reduced (active) AniA concentrations are modelled by this equation

$$\frac{d[A_a]}{dt} = m_3([A] - [A_a])[E] - m_1[NO_2^-][A_a]$$



and reduced (active) NorB concentrations are modelled by this equation

$$\frac{d[B_a]}{dt} = l_3[Q_a]([B] - [B_a]) - l_1[NO][B_a]$$



By keeping the quantities involved in their original state and not making any assumption about time-scale separation I am able to make predictions regarding the transient oxidation states of the various components. These are potentially experimentally accessible and appear to be crucial for the dynamic response of the chain in different environments.

The model contains no implied information about cell density. This means the values for various component concentrations will differ between experiments. Initially the optical density of cultures was used to determine the cell density however experiments proved that this was not a completely reliable proxy for cell density as this also includes dead cells. Using optical density as a cell density proxy should have given linear relations between cell densities and reaction rates, however this proved not to be the case, with rates of oxygen reduction different between cultures with the same optical density. Therefore where possible, any normalisation that was carried out used the initial oxygen reduction rate as a relative indicator.

### 3.1.2 Assumptions and their Justifications

I have made a number of assumptions regarding the kinetics and reactions taking place in the model.

1. **I have assumed that NO inhibits the reduced  $cbb_3$  and not the oxidised form, since I wouldn't expect Nitric oxide to bind to an inactive enzyme.**  
This is corroborated by Giuffre et al.<sup>88</sup>, who show significant levels of inhi-



bition of reduced cytochrome. They do also however observe low levels of inhibition of the oxidised enzyme also. Their experiments used cytochrome c oxidase (aa3) rather than *cbb<sub>3</sub>*, but I believe this assumption still stands as the enzymes are of the same family.

2. **No backwards reactions.**

3. **No Michaelis-Menton kinetics.** Cannot assume that time-scales are separated as the rates of intermediate reaction steps are not known.

4. **All cytochromes can be modelled as one.**

5. **Laz and *c<sub>5</sub>* effects on AniA and *cbb<sub>3</sub>* respectively can be ignored.** They are not the prime electron donors to their terminal reductases and contribute very little overall to the reduction<sup>22</sup>.

### 3.2 Parameters and their Prior Distributions

None of the rate constants or concentrations which were required for this model have previously been determined for *Neisseria meningitidis*, so values from other similar organisms had to be used instead. In some cases there appears to be no data in the literature regarding values of particular components. Table 3.1 lists the values that have been obtained from the literature.

#### Variables

##### O<sub>2</sub> - Oxygen concentration

This variable is always obtained directly from the experimental dataset as it indicates the starting point for oxygen in the model. It is always set to the first oxygen data point in the dataset and has no prior distribution. It is usually a fixed value, except in cases where the dataset indicates measurement artefacts.

Symbol	Description	Value
$k_1$	Rate of $O_2$ reduction by reduced $cbb_3$	$415 \mu M^{-1} s^{-1}$
$k_3$	Rate of $cbb_3$ reduction by cytochrome pool	$3 \mu M^{-1} s^{-1}$
$l_1$	Rate of NO reduction by reduced NorB	
$l_3$	Rate of NorB reduction by quinone pool	
$m_1$	Rate of $NO_2^-$ reduction by reduced AniA	
$m_3$	Rate of AniA reduction by cytochrome pool	$4.8 \pm 0.2 \mu M^{-1} s^{-1}$
$k_5$	Rate of $cbb_3$ inhibition by NO	$10^8 M^{-1} s^{-1}$
$k_6$	Rate of recovery of NO inhibited $cbb_3$	
$\beta$	Rate of passive diffusion in of $O_2$	
$K_O$	Saturation $O_2$ level	$126 \mu M$
$g$	Rate of electrons in from NADH	
$f$	Rate of reduction of cytochromes by quinones	
$\gamma$	Spontaneous loss of NO	
$Q$	Concentration of quinones	$0.3 \mu M$
$X$	Concentration of cytochromes	$4000 \text{ nM} - cbb_3$
$A$	Concentration of AniA	
$B$	Concentration of NorB	
$C$	Concentration of $cbb_3$	$30 \text{ nM}$

Table 3.1: Model parameters

### NO - Nitric oxide concentration

As for Oxygen concentration, this variable is simply obtained from the dataset and the same conditions apply.

### $NO_2^-$ - Nitrite concentration

Nitrite concentration is also handled in the same way as the oxygen and nitric oxide concentrations.

### E - Reduced cytochrome concentration

Unknown at start of simulation. Assume close to zero, and certainly less than total. The best prior to use would be the value after a couple of simulation seconds, however this would no longer be a prior.

#### **A<sub>a</sub> - Reduced AniA**

Unknown at start of simulation. Assume close to zero, and certainly less than total. The best prior to use would be the value after a couple of simulation seconds, however this would no longer be a prior.

#### **B<sub>a</sub> - Reduced NorB**

Unknown at start of simulation. Assume close to zero, and certainly less than total. The best prior to use would be the value after a couple of simulation seconds, however this would no longer be a prior.

#### **C<sub>a</sub> - Reduced *cbb*<sub>3</sub>**

Unknown at start of simulation. Assume close to zero, and certainly less than total. The best prior to use would be the value after a couple of simulation seconds, however this would no longer be a prior.

#### **C<sub>X</sub> - Reversibly NO inhibited *cbb*<sub>3</sub>**

Unknown at start of simulation. Assume close to zero, and certainly less than total. The best prior to use would be the value after a couple of simulation seconds, however this would no longer be a prior.

#### **Q<sub>a</sub> - Reduced Quinones**

Unknown at start of simulation. Assume close to zero, and certainly less than total. The best prior to use would be the value after a couple of simulation seconds, however this would no longer be a prior.

#### **Parameters**

##### **k<sub>1</sub> - Rate of O<sub>2</sub> reduction by reduced *cbb*<sub>3</sub>**

Preisig et al.<sup>23</sup> show that *B. japonicum cbb*<sub>3</sub> (*fixNOQP*) has a  $K_m$  of  $55.7 \pm 24.2$  nM O<sub>2</sub>, and  $V_{max}$   $37.4 \pm 9.2$  nmolO<sub>2</sub>min<sup>-1</sup>mg<sup>-1</sup>.

Given  $v = \frac{V_{max}[S]}{K_m + [S]}$  Then at high  $O_2$  rate is:  $v = \frac{37.4 \times 100,000}{55.7 + 100,000} = 37.4 \text{ nmol}^{-1} \text{ min}^{-1} \text{ mg}^{-1} = 0.000622986 \text{ } \mu\text{mol}^{-1} \text{ s}^{-1} \text{ mg}^{-1}$

A value for  $k_1$ , was calculated by using the  $K_{cat}$  value from *Pseudomonas stutzeri*<sup>89</sup>, and the  $k_m$  value from *Neisseria lactamica*<sup>90</sup>, which are  $166 \text{ s}^{-1}$  and  $0.4 \text{ } \mu\text{M}$  respectively.  $k_1$  can be calculated as  $\frac{166 \text{ s}^{-1}}{0.4 \text{ } \mu\text{M}} = 415 \text{ } \mu\text{M}^{-1} \text{ s}^{-1}$ .

### **$k_3$ - Rate of $cbb_3$ reduction by cytochrome pool**

This was calculated from values obtained from the maximum reduction rate of  $cbb_3$  by cytochrome  $c_4$  in *Vibrio cholerae*<sup>55</sup>. A rate of 300 electrons transported per second was observed with a cytochrome  $c_4$  concentration of  $100 \text{ } \mu\text{M}$ . This concentration was not saturating, but there appears to be a linear relationship between rate and concentration. I assume that 1 electron equals 1 reduction of  $cbb_3$ , thus the rate of reduction of  $cbb_3$  by cytochromes is  $\frac{300 \text{ s}^{-1}}{100 \text{ } \mu\text{M}} = 3 \text{ } \mu\text{M}^{-1} \text{ s}^{-1}$ .

### **$l_1$ - Rate of NO reduction by reduced NorB**

240 and 256 nanomoles NO reduced per minute per OD600 unit Barth et al.<sup>40</sup>.

This needs fixing. 50% dry weight, rather than 15% wet weight.

Observed rates of NO reduction by Rock et al.<sup>29</sup> give  $54 \pm 6 \text{ nmol min}^{-1} \text{ mg}^{-1}$ . This is in whole cells however.  $\approx 10 \text{ nmols}^{-1}$  in an  $OD_{600} = 1$  culture. Converting to molar gives  $2 \text{ } \mu\text{Ms}^{-1}$ .

### **$l_3$ - Rate of NorB reduction by quinone pool**

Benchmark estimate is somewhere around about  $1 \text{ } \mu\text{M}^{-1} \text{ s}^{-1}$ .

### **$m_1$ - Rate of $\text{NO}_2^-$ reduction by reduced AniA**

### **$m_3$ - Rate of AniA reduction by cytochrome pool**

This value is the observed electron transfer rate between the equivalent cytochrome and nitrite reductase from *Achromobacter xylosoxidans*. A value of  $4.8 \pm$

$0.2 \mu M^{-1}s^{-1}$  was observed during stopped-flow experiments<sup>91</sup>.

#### **$k_5$ - Rate of $cbb_3$ inhibition by NO**

Giuffre et al.<sup>88</sup> and Blackmore et al.<sup>92</sup> showed with cytochrome *c* oxidase that NO could bind reversibly and inhibit the activity of the enzyme. The rate they calculated was  $10^8 M^{-1}s^{-1}$ . I assume that even though the enzyme is different, its NO binding characteristics would be similar to that of  $cbb_3$  as it is of the same family.

#### **$k_6$ - Rate of recovery of NO inhibited $cbb_3$**

Giuffre et al.<sup>88</sup> calculated a half-life of  $t_{1/2} \approx 80$  min.

$K_d$  from Rock et al.<sup>29</sup> was calculated to be about 500 nM, which tallies with values from  $k_5$  and  $k_6$ .

#### **$\beta$ - Rate of passive diffusion in of $O_2$**

This value is highly dependent on the culture, and is in some way tied to the density of the culture, however the relationship is not known. During early experiments I noticed that oxygen diffusion was slower in high density cultures compared to those of low density, experiments to examine the relationship proved fruitless in determining any relationship. In addition this parameter is a product of the experimental set-up rather than the model itself.

#### **$K_O$ - Saturation $O_2$ level**

This value is dependent on the particular culture being modelled, however it's prior value is usually set to  $126 \mu M$  as this figure was observed during experiments to determine oxygen diffusion rates into the culture.

**g - Rate of electrons in from NADH (or rate of reduction of quinones)****f - Rate of reduction of cytochromes by quinones**

Snyder et al.<sup>50</sup> showed by reducing yeast cytochrome  $bc_1$  by using 25  $\mu\text{M}$  menaquinol the rate constants were  $7.9 \text{ s}^{-1}$  for cytochrome b, and  $1.55 - 6.9 \times 10^5 \text{ M}^{-1}\text{s}^{-1}$  for cytochrome  $c_1$  (second order).  $0.155 - 0.69 \mu\text{M}^{-1}\text{s}^{-1}$ .

 **$\gamma$  - Spontaneous loss of NO****Q - Concentration of quinones**

This value was calculated based on data from Hedricks et al<sup>93</sup>. The protein content of the cells was assumed to be similar to that of *E. coli* at 15% of wet weight, where each cell weighed 2 pg, and that there were 1  $\mu\text{mol}$  of respiratory quinones per g of bacterial protein. A culture of *Neisseria meningitidis* with  $OD_{600} = 1$  has  $1 \times 10^9$  cells/ml, therefore there are 1.5 nmol of quinones in 5 ml culture ( $5 \times 10^9 \text{ cells} \times 2 \times 10^{-12} \text{ g} \times 15\% \times 1 \mu\text{mol/g}$ ), converted to molarity is 0.3  $\mu\text{M}$ .

**X - Concentration of cytochromes**

Manu's thesis<sup>22</sup> suggests total cytochrome concentration (inc. *cbb<sub>3</sub>*) to be about 4000 nM.

**A - Concentration of AniA**

No idea, probably need to guess based on cell volume (0.6-1.0  $\mu\text{m}$  diameter, no useful ref), 10% of cell volume being membrane, and number of proteins in membrane.

**B - Concentration of NorB**

No idea, probably need to guess based on cell volume (0.6-1.0  $\mu\text{m}$  diameter, no useful ref), 10% of cell volume being membrane, and number of proteins in membrane.

### C - Concentration of *cbb<sub>3</sub>*

No idea, probably need to guess based on cell volume (0.6-1.0  $\mu\text{m}$  diameter, no useful ref), 10% of cell volume being membrane, and number of proteins in membrane.

*cbb<sub>3</sub>* is probably 0.1-1% of cell protein. 10% of cell is membrane. 15  $\mu\text{g}$  in 5 ml based on numbers from Q above. *cbb<sub>3</sub>* is approximately 100 kDa in molecular weight. Converting to molarity gives a concentration of approximately 30 nM.

### 3.3 Solving Ordinary Differential Equations

The model equations (given in Chapter 3 [Model - Construction and Parameters]) are solved in parallel using the common 6<sup>th</sup> order Runge-Kutta-Fehlberg algorithm for integrating ordinary differential equations<sup>94</sup>. Adaptive step-sizes were implemented using the Cash-Karp method<sup>95</sup>. The adaptive step size system was required as it prevented the introduction of systemic numerical instabilities.

The parameter estimation system and ODE solver were a bespoke implementation written in Java. The Runge-Kutta algorithm was modified from that found in Numerical Recipes in C<sup>96</sup>. I decided to write a custom implementation rather than using off the shelf systems for solving ODEs and parameter estimation as I wanted the greatest flexibility in how I integrated the two techniques, and it allowed me to quickly and easily tailor the code to my needs. Initially I tried using COPASI<sup>77</sup>, however at that time it had limitations that I could not overcome, such as bulk addition of components at arbitrary time-points.

The implementation of the model has no constraints on respiratory substrate concentration, thus allows the altering of these concentrations whilst solving the equations, however changes to substrate concentration have to be made programmatically to inform the model of the change (`if (t == 50) then NO_conc += 20;`). This ability means that the switch between aerobic and anaerobic respiration can be examined synthetically, and the model is also capable of simulating how the respiratory system responds to addition of substrates such as Nitric Ox-

ide. This ability was an absolute requirement, as in order to fully parametrise the model it was necessary to isolate sections of the model, which required adding aliquots of respiratory substrate during respiration.

### **3.4 Parameter Estimation**

Estimating the parameter values for the components in the mathematical model involved comparing the biological results with those produced by solving the ODEs and adjusting the parameter values to minimise the difference between the two results. The different methods for parameter estimation that I investigated are detailed in Chapter 4 [Parameter Estimation Methodologies].



## Chapter 4

# Parameter Estimation Methodologies

Below are the various different methods for parameter estimation that I investigated during the course of this work. All of these methods involve a sampling system that attempts to select parameter values which minimise the difference between the simulation result and the experimental data by calculating a *fitness value*. The aim of the parameter estimation methodology was to get this *fitness value* as close to zero (perfect fit/no difference) as possible. Two different calculations were used to create the *fitness value*. One was the sum of the Least Squares Differences between the measured components in the experimental data and the simulation result. This was used in early parameter estimation runs.

$$f = \sum_{j=1}^n \left( \sqrt{\sum_{i=1}^m (\Delta x_{ij})^2} \right) \quad (4.1)$$

The second method for calculating the *fitness value* was a lognormal correlation which allowed greater tuning, as the standard deviation of the distribution could be set to adjust how much fitter the simulation result needed to be to be accepted.

$$f = \sum_{j=1}^n \left( \sum_{i=1}^m \left( \ln \left( \frac{1}{2\pi\sigma_j^2} e^{-\frac{(0-0)^2}{2\sigma_j^2}} \right) - \ln \left( \frac{1}{2\pi\sigma_j^2} e^{-\frac{(x_{ijFIT} - x_{ijDATA})^2}{2\sigma_j^2}} \right) \right) \right) \quad (4.2)$$

In most cases the components used for calculating the *fitness value* are Oxygen and Nitric Oxide, as these were the primary measured chemicals.

The main difference between the parameter estimation methodologies laid out below are the ways in which they generate new parameter values, either from a probability distribution or based on the previous value, and the way this is applied and tested against the experimental data.

### Monte Carlo Methods

I include a brief section here to describe Monte Carlo Methods, as the techniques I used for parameter estimation all use this method as their estimator in some form. “Monte Carlo Methods” is a generalised term to describe a stochastic technique that makes use of random numbers to examine a problem in conjunction with probability statistics. Monte Carlo Methods allow us to model complex systems without having to exhaustively search every possible outcome. Large systems are sampled in random configurations and that data applied in such a way that it can be used to describe the system as a whole. “Monte Carlo techniques are often the only practical way to evaluate difficult integrals or to sample random variables governed by complicated probability density functions”<sup>97</sup>.

#### 4.1 Simulated Annealing

This technique was described independently by Kirkpatrick et al.<sup>98</sup> and Černý<sup>99</sup>. The name comes from the metallurgical annealing process whereby large crystals are formed while a material is slowly cooled. The slow cooling increases the probability of individual crystals obtaining lower energy states than the ini-

```
c1 <- c0;
c2 <- mutate(c1);
i <- 0;
while i < i_max
  if fitness(c1) > fitness(c2)
    c2 <- mutate(c1)
  else
    c1 <- mutate(c2)
  i <- i + 1
if fitness(c1) > fitness(c2)
  return c1
else
  return c2
```

Figure 4.1: **Pseudo-code showing how the simplest annealing algorithm works.**

tial. As the material cools the “distance” each crystal can move along the energy landscape decreases. Simulated annealing “consists of a discrete-time inhomogeneous Markov chain”<sup>100</sup> whereby the previous state is modified with a perturbation kernel (the neighbouring states) and then accepted or rejected using a transition probability which depends on the current temperature and the energies of the previous and current states. The advantage of this scheme is that areas of local minima have a lesser effect on the outcome of the Markov chain as the high initial temperature allows for the chain to “jump” out of this minima.

Figure 4.1 contains some simple pseudo-code which shows how the basic algorithm works (without the annealing temperature). This will provide a “best” parameter set, but there is no information about the possible spread of values in the parameter set. Given that it is unlikely that a single point-value parameter-set solution exists that will accurately describe the system it is necessary to produce a spread of results that will adequately describe the system instead. To this end I used a modified version of simulated annealing integrated with aspects of a simple genetic algorithm. In the genetic algorithm paradigm a synthetic “chromosome” is created containing which contains “genes” representing the parameters in the simulation. These include the rate constants, concentrations of various components and initial concentrations of substrates and products. This chromosome is then copied and perturbed several times (depending on the eventual

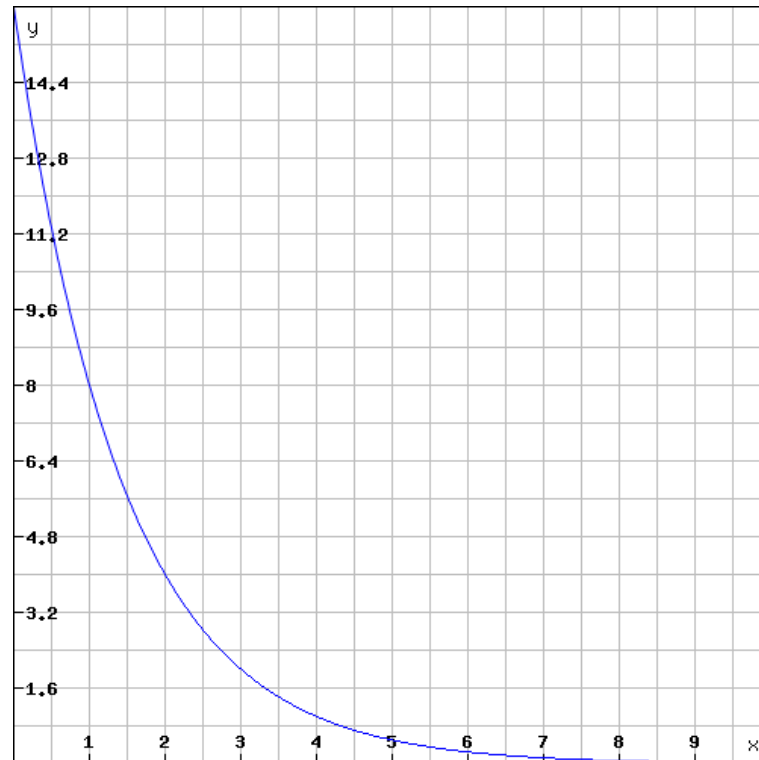


Figure 4.2: **Example simulated annealing temperature schedule.** This represents how the annealing temperature changes as the annealing process progresses. Temperature is denoted by the y-axis value, and simulation progress by the x-axis value. This is a heavily compressed time-frame, as in reality the system would normally process 10,000 sets of parameters at each annealing temperature.

population size required), with the size of the perturbation being dependent on the current annealing temperature. For instance the highest temperature could indicate that the individual parameters can be perturbed by up to  $\pm 10\%$ , and as the temperature decreases the perturbation percentage has a concomitant decrease. An example annealing temperature schedule is shown in Figure 4.2. The annealing temperature is programmed to decrease after a defined number of iterations such that the magnitude of individual mutations becomes smaller as the simulation progresses. This should have the effect of honing in on a set of parameters with high fitness. Once the chromosome population has been created, 2 are selected at random and their fitnesses evaluated, in this case by the Least Squares Difference method. The chromosome with the higher *fitness value* is discarded and the other is cloned and perturbed. The two chromosomes are then added back to the chromosome population. The genetic algorithm is used to

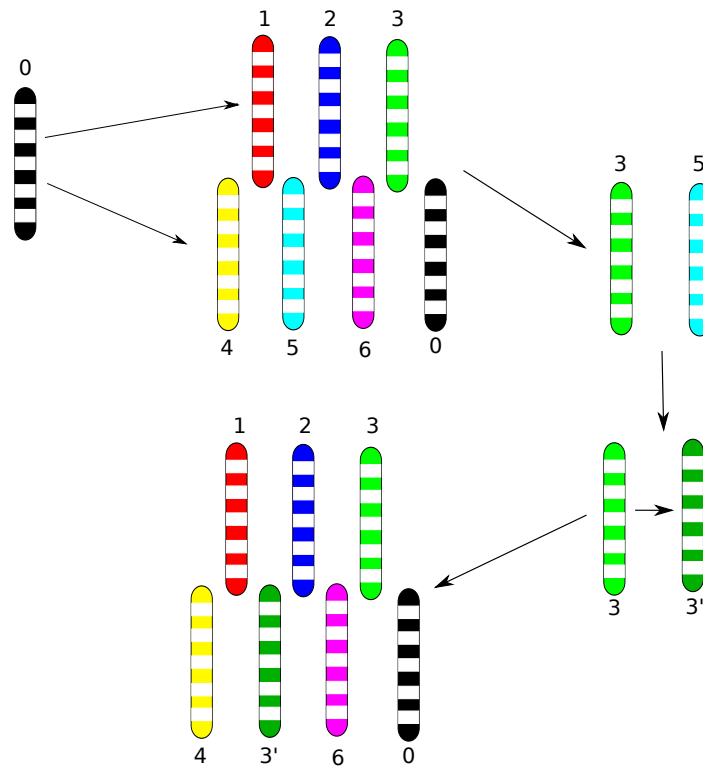


Figure 4.3: **Schematic diagram showing the technique used to generate a spread of parameters using a synthetic chromosome.** The parameters are loaded as genes on the chromosome which are then perturbed, 2 chosen and the fittest kept and perturbed. Each time a chromosome is perturbed it is reintroduced into the chromosome pool, and the next 2 chromosomes are chosen at random.

improve the parameters sets by perturbing genes (individual parameters) from fit chromosomes (complete parameter sets), re-running the simulation and discarding unfit parameter sets. An unfit parameter set is defined as one with an *fitness value* lower than the best so far. This technique involves having two chromosomes selected at any one time. The parameters from each chromosome are simulated and the least fit one is discarded. At this point the contents from the fitter chromosome are cloned and perturbed, and the cycle is repeated. Figure 4.3 shows this diagrammatically. After many cycles (upwards of 1000) the chromosome pool should only contain the best fitting parameter sets to the experimental data. The spread of the parameters can be used to infer the sensitivity of the simulation to changes in parameter values in a similar way to that described by Toni et al.<sup>101</sup>.

### Advantages

- Easy to implement.
- Can avoid local energy minima by jumping when the temperature is high.
- Energy need only be calculated for 2 samples at any one time.
- High optimisation performance on some problems.

#### **Disadvantages**

- Slow performance on certain problems.
- Cannot produce probability distributions.

#### **Reason(s) for rejection**

- Seemed to be incapable during testing of settling on solutions to Nitric Oxide reduction datasets.
- No probability distributions which were eventually required to incorporate data from previous datasets.

### **4.2 Approximate Bayesian Computation by Sequential Monte Carlo**

“Approximate Bayesian Computation methods have been conceived with the aim of inferring posterior distributions where likelihood functions are computationally intractable or too costly to evaluate. They exploit the computational efficiency of modern simulation techniques by replacing calculation of the likelihood with a comparison between the observed data and simulated data”<sup>101</sup>.

To incrementally improve the parameter sets, a version of Bayesian inference is used in conjunction with a standard Monte Carlo method in a system called Approximate Bayesian Computation by Sequential Monte Carlo (ABCSMC) as described by Toni et al.<sup>101</sup>. An implementation of algorithm (S) was used from that paper.

**Bayesian Inference** - This is a statistical method for inferring the probability of a hypothesis based on available evidence. As more evidence is accumulated, the

inference is updated and the probability of the hypothesis being true is changed. Given enough evidence, the probability of the hypothesis being true should either be very high or very low causing you to either accept or reject the hypothesis. Bayesian inference relies on having a prior probability (or probability distribution) for the hypothesis, and this can inevitably introduce a level of bias into the inference. Bayesian inference can be described thus:

$$P(H | E) = \frac{P(E | H)}{P(E)} \cdot P(H) \quad (4.3)$$

- $P(H | E)$  is the posterior distribution of  $H$  given  $E$ .
- $P(H)$  is the prior distribution
- $\frac{P(E | H)}{P(E)}$  is the impact of  $E$  on the degree of belief in  $H$ .

A simplistic example of using Bayesian inference to alter a hypothesis could happen in the case of having two jars of sweets. Jar 1 has 15 strawberry sweets and 25 raspberry sweets. Jar 2 has 20 of each. Supposing a third party selects 1 sweet at random from 1 of the jars. They select a strawberry sweet, what is the probability that it came from Jar 1? From the point of view of our third party both jars are identical, therefore  $P(H_1) = P(H_2)$  and the total probability must equal 1, so the prior probability of each jar is 0.5. The observation,  $E$  is of a strawberry sweet, which we can then use to calculate the likelihood of it being from each jar individually by  $P(E | H_1) = 15/40 = 0.375$  and  $P(E | H_2) = 20/40 = 0.5$ . Bayes formula can then be used to work out the probability of the strawberry sweet being from jar 1, that is  $P(H_1 | E)$ .

$$\begin{aligned}
 P(H_1 | E) &= \frac{P(E | H_1)P(H_1)}{P(E | H_1)P(H_1) + P(E | H_2)P(H_2)} \\
 &= \frac{0.375 \times 0.5}{0.375 \times 0.5 + 0.5 \times 0.5} \\
 &= 0.429
 \end{aligned} \tag{4.4}$$

Before the observation of the sweet, the probability of the third party taking from jar 1 was the prior probability of 0.5. After the observation this probability must be revised to 0.429.

Bayesian inference is widely used in computational analysis for artificial intelligence and email spam identification. It is also used in the field of population genetics and phylogenetics<sup>102</sup>.

**Approximate Bayesian Computation** - This is an adaptation of Bayesian inference which allows approximately the same inferences to be made, with considerably less computation. It operates on representations of the datasets rather than the datasets themselves. Common examples are population mean and variance. This is useful for large complex datasets where the probability of a simulation of the dataset matching the original is very small (unacceptably so), in this case a representation of the datasets can be used, and the difference calculated. If the difference is less than a pre-defined acceptance threshold, then the simulated dataset is accepted. ABC originally came from the fields of population and evolutionary genetics<sup>103</sup>, but are now being applied to complex and stochastic dynamical systems<sup>101,104,105</sup>.

ABC differs from standard Bayesian inference shown in Equation 4.3 in that the likelihood term does not need to be calculated. Instead the difference between the summary statistics of the observed data and the simulated data is used. The simulated data is considered a true sample from the posterior distribution if the



difference in summary statistics is less than a predefined acceptance threshold.

The most basic ABC methods takes the following form:

$\theta$  is a parameter vector to be estimated,  $\pi(\theta)$  is the prior probability distribution, and  $x$  is the observed data. The posterior distribution is  $\pi(\theta | x) \propto f(x | \theta) \cdot \pi(\theta)$ .

1. Create a candidate parameter vector  $\theta^*$  from the prior distribution  $\pi(\theta)$ .
2. Simulate dataset  $x^*$  using the model and parameter vector  $\theta^*$ .
3. Compare  $x^*$  with  $x$  using a distance function  $d$  and an acceptance criteria  $\epsilon$ .  
If  $d(x, x^*) \leq \epsilon$ , accept  $\theta$ .

Given a low enough value for  $\epsilon$ , the output distribution should approximate the true posterior distribution if sampled a large enough number of times.

**Sequential Monte Carlo** - This is a method of particle filtering whereby a large set of samples ( $N$ ) are drawn from the prior distribution, and for each sample, the probability is calculated. Weights for each particle are assigned based on the probabilities, and these affect how likely a particle is to be selected in subsequent rounds of selection. At the end of each round, the posterior distribution, that of the  $N$  particles becomes the prior distribution for the next round.

**Approximate Bayesian Computation by Sequential Monte Carlo** - This combines the previous two methods by drawing a large number of particles from the prior distribution using Bayesian inference. The prior distribution is discrete in the scheme used here, so a perturbation kernel based on a laplacian or gaussian distribution is used on each sample to provide small deviations to better approximate a continuous prior distribution. Each sample is simulated and only accepted if it exceeds the acceptance threshold. This is calculated based on the least-squares difference (LSD) between the simulated data and the original dataset. If a sample is rejected, a new one is drawn from the prior distribution and SMC then continues as described above. The weights of the accepted samples are calculated based on the probabilities of being selected from the prior and the samples go on to form the posterior distribution. For each subsequent round,

the mean LSD of the posterior distribution from the previous round is used as the acceptance threshold. This ensures that each round results in better fitting parameter sets. The cycle is then repeated until a pre-defined cycle limit is reached<sup>101</sup>.

A significant advantage of this technique is that it is readily parallelisable, as each particle in the SMC process is independent, thus can be simulated in parallel. A parallel version of this algorithm was implemented in the JAVA programming language which resulted in significant speedups when multiple processing threads can be used. The threading manager means that the algorithm is theoretically most efficient (in terms of computational time) when the number of particles is an exact multiple of the number of processing threads. In practice however this is negated by the fact that some particles require multiple samples due to them not meeting the acceptance criteria.

#### **Advantages**

- Paralellisable. Leading to improved performance on multiprocessor systems.

#### **Disadvantages**

- Requires a suitable distance function or summary statistic.

#### **Reason(s) for rejection**

- Seemed incapable of settling on sensible posterior distributions with some datasets. I suspect the distance function used was causing a conflict which meant the algorithm was accepting bad parameter sets and rejecting good ones.

### **4.3 Metropolis Hastings Monte Carlo**

The Metropolis-Hastings algorithm is Markov Chain Monte Carlo method to retrieve sequences of random samples from a probability distribution which cannot be sampled directly (or would be very difficult) such as when no probability distribution function exists. The algorithm was originally developed by Metropolis

et al.<sup>106</sup> for generating samples from the Boltzmann distribution. It was later extended to a more general form for any distribution by Hastings<sup>107</sup>.

MHMC allows each individual parameter to follow a biased random walk until it reaches a point of maximum “fitness.” The typical output of this algorithm is a set of parameter trajectories which begin with a “burn in” period, followed by a parameter distribution. The “burn in” period contains data that is discarded, as it does not form part of the target distribution. The length of this burn in period often varies depending on how far the starting samples are from the target distribution. The parameter distribution can be calculated from the data that is left after the burn in period. This is done by a simple statistical analysis of the resulting data points. Since the distributions cannot easily be described as functions, the data are transformed into histograms with a set bin width. These histograms can be read and used as priors for subsequent runs of the MHMC algorithm.

The MHMC algorithm has been validated initially by using a much simpler ODE system than is required by the respiration model. A Lotka-Volterra system was used as this can be solved much more quickly by virtue of having far fewer parameters (4 as opposed to >20). The Lotka-Volterra system describes a simple predator-prey relationship and only requires two first-order, non-linear differential equations, which are shown in equation 4.5.

$$\begin{aligned}\frac{dx}{dt} &= x(\alpha - \beta y) \\ \frac{dy}{dt} &= -y(\gamma - \delta x)\end{aligned}\tag{4.5}$$

Validation of using this system required a simulated dataset with known parameter values to be produced. This dataset then forms the input for the MHMC algorithm which will try and obtain those same parameter values. Given the simplicity of this system, a particularly bad set of initial parameter estimates was

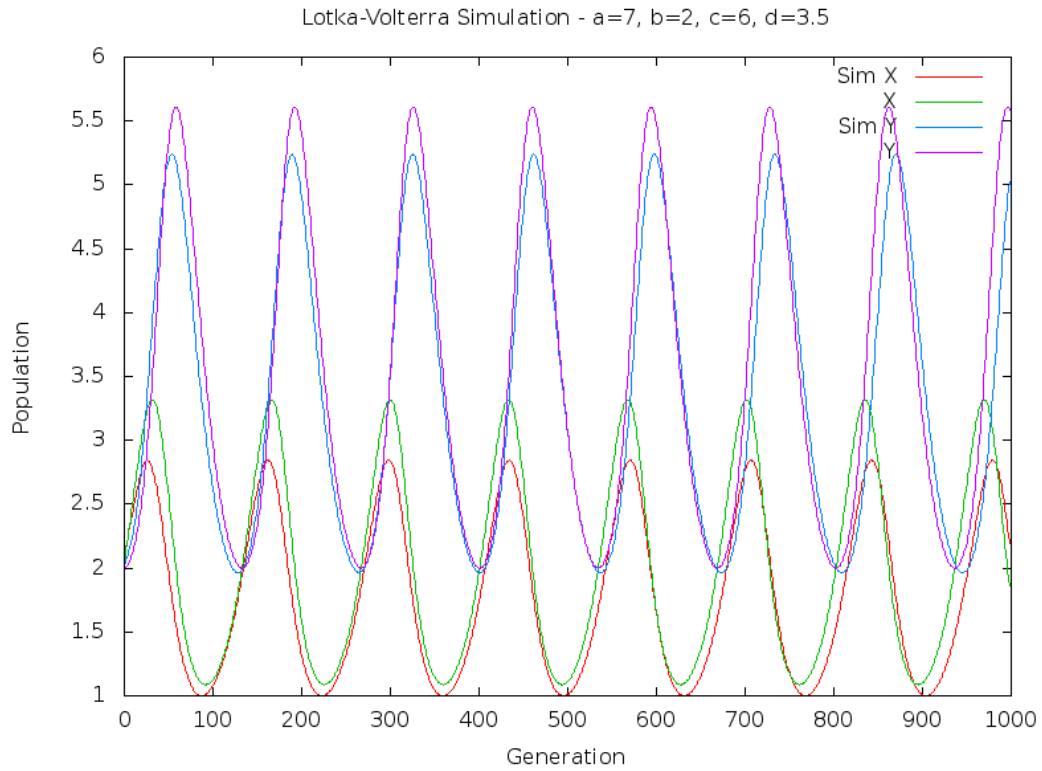


Figure 4.4: **Simulation results of the Lotka-Volterra validation run.**

given to exaggerate the burn in period, and to show that given a long enough time the simulation will eventually settle on “correct” values. This validation step also informs the likely values for two tuning variables in the algorithm; the *acceptance* - how stringent the algorithm is on accepting new parameter sets, and the *sigma* value - this describes the magnitude of parameter perturbation at each iteration. The graphical results of the Lotka-Volterra validation are shown in figures 4.4 and 4.5.

#### 4.4 Implementation

The initial parameters used to solve the equations were a set of priors based on preliminary experimental results. These parameters only provide a starting point as the second stage of computation involves modifying the parameters in order to provide a better fit against experimental data. To incrementally improve the parameter sets, a version of Bayesian inference is used in conjunction with a standard Metropolis-Hastings Monte-Carlo method.

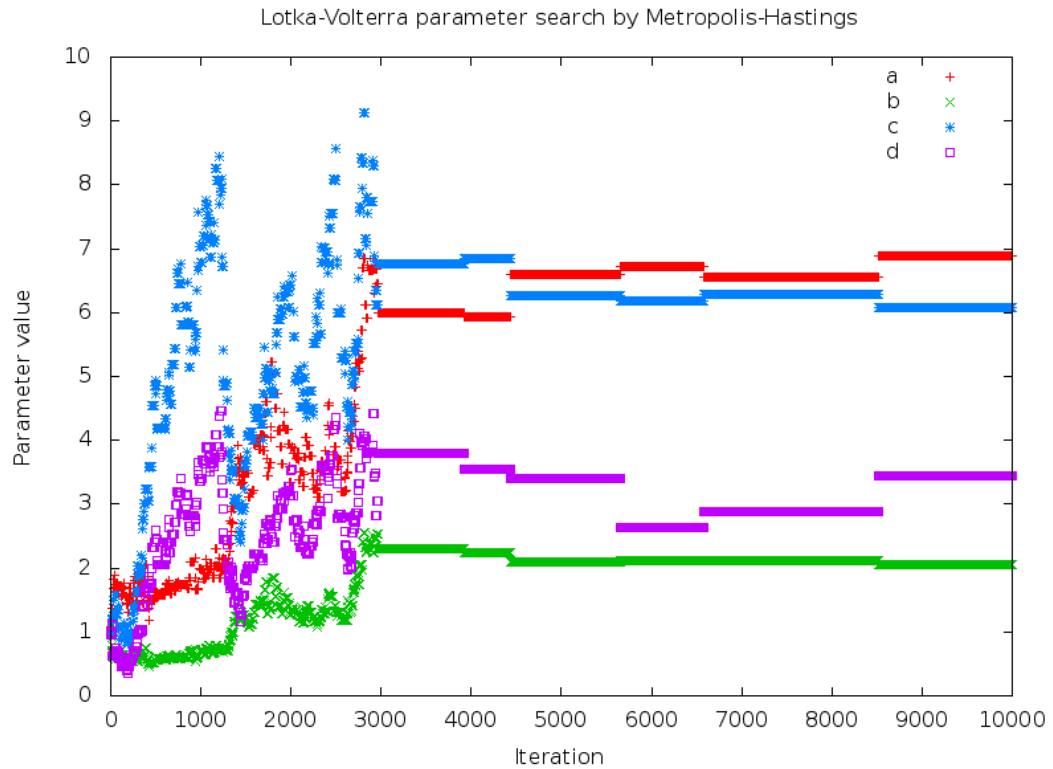


Figure 4.5: **MHMC results of the Lotka-Volterra validation run.** Note the initial burn-in period followed by the distribution trajectory.

I used Bayesian inference to inform the simulation parameters for a particular dataset based on prior probability distributions. These distributions were obtained as output from a previous dataset. I integrated this with a Metropolis-Hastings algorithm for sampling the prior probability distributions. Each parameter was sampled, and the parameter set was used to solve the ODE model. Based on the fitness output of the solved model, the Metropolis-Hastings algorithm allows parameters to be modified in a biased random walk which ultimately leads them to their most fit state, calculated using Log Normal probability.

#### Advantages

- 

#### Disadvantages

-

#### 4.5 Integrative Scheme

*Currently copied verbatim from paper*

In order for us to iteratively generate a parameter set we needed to separate the model into simpler units whereby we can obtain data about a specific set of variables. We did this so that the simplest part of the model was parametrised first. In this case it was oxygen respiration, which only requires one enzyme (although it does still require the electron transport chain). This section of the model also has the simplest experimental dataset. After parametrisation, a new section of the model was introduced, with its associated experimental dataset.

Experimental data was gathered for the first dataset, and this is used as a training set, with almost flat priors based on preliminary experimental data. The data was pre-processed and normalised if necessary and then presented to the Bayesian Parameter Estimation system. The MHMC algorithm samples from the prior distribution and then uses those samples as parameters to solve the model. It aims to improve the calculated fitness value and is ordinarily run for at least 100,000 iterations to give the system time to settle on the fittest parameters. The system is run on the same dataset 10 times to generate statistically significant results. The eventual output of the MHMC runs are posterior probability distributions for each of the parameters in the model. In accordance with Bayesian inference these are then used as prior distributions.

At this point the next section of the model to be parametrised is decided, the appropriate experimental data identified and obtained, and the process is repeated until the entire model has been populated. The final result should be a set of reasonably narrow probability distributions for each of the parameters which describe the system accurately enough to correctly predict the behaviour of the system *in vivo*.

# Chapter 5

## Oxygen Reduction in *N. meningitidis*

### 5.1 Aerobic Reduction of Oxygen

Modelling oxygen reduction was the simplest both experimentally and mathematically. MC58 cultures were grown in aerobic conditions for around 3 hours, or until the OD<sub>600</sub> had reached 0.3-0.9. Cultures were then transferred to the electrode chamber and the oxygen concentration was recorded as the culture respired. Once the culture had become anaerobic it was re-aerated by bubbling air through the culture with a sterile pasteur pipette. This restored oxygen levels throughout the culture and they began respiring oxygen once more.

In the model, oxygen reduction is described by equation (1) which is the change in oxygen concentration over time. Modelling the reaction also requires equations (4-6) also to describe the flow of electrons into the system and to the terminal reductase. This involved 17 parameters and variables to be estimated.

The experimental dataset shows that oxygen reduction in *Neisseria meningitidis* is a simple linear system with the reductase having a high affinity for oxygen demonstrated by the almost complete lack of non-linearity as oxygen concentration approaches zero. This apparent simple linearity could be modelled with a high degree of accuracy with just 2 parameters in a simple  $y = -mx + c$  system. However this does mean that the posterior distributions generated are very wide and therefore allows much greater freedom for the next dataset to explore the

parameter space.

The final solved output of the parameter estimation for this dataset can be seen in Figure 5.1. The initial parameter set used to start the Monte-Carlo run was one based on some preliminary experimental data (dataset not shown) and priors from literature about sensible concentrations and rate constants for this system. Very little information is readily available in the literature to populate the model.

Given our knowledge of the underlying transport chain and the affinity of *cbb<sub>3</sub>* for oxygen, we expect a linear reduction of oxygen with high affinity over nearly two orders of magnitude. It is however remarkable that we can model this behaviour with so few components in the model, as it requires significant changes in the reduction state of the enzymes to achieve this.

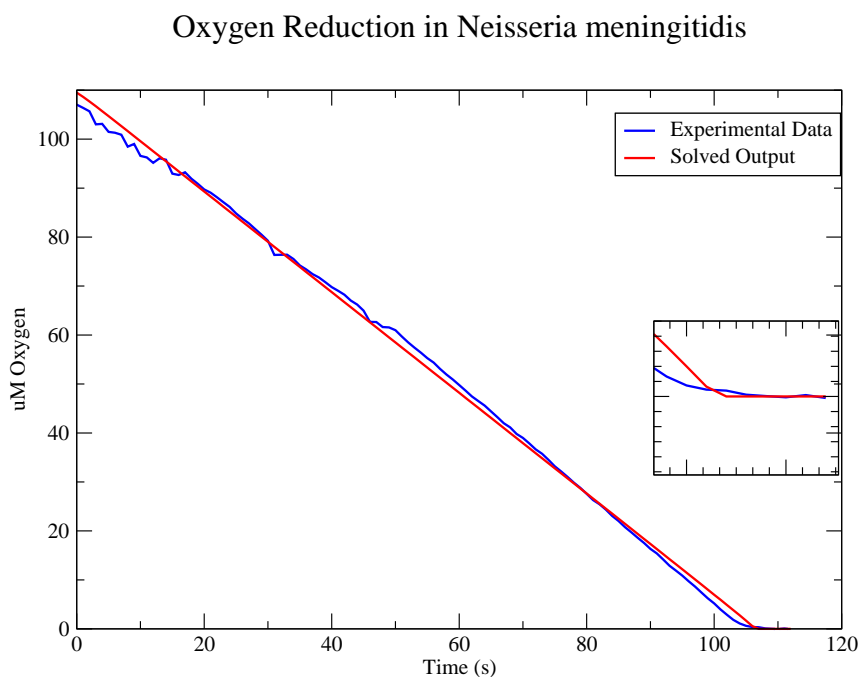


Figure 5.1: **Oxygen Reduction in *Neisseria meningitidis*.** This dataset shows the simple linear reduction of Oxygen in aerobic conditions. The high affinity of *cbb<sub>3</sub>* for oxygen is evidenced by very little non-linearity at low oxygen concentrations. The solved output is a representative result of the parameter estimation system.



**5.1.1 Introduction**

**5.1.2 Results**

**5.1.3 Discussion**

## Chapter 6

# Nitric Oxide Reduction in *N. meningitidis*

Modelling nitric oxide reduction involves adding nitric oxide whilst cultures are respiring aerobically. The conditions are the same as for oxygen reduction, except that nitric oxide solution is added to a concentration of  $\approx 5 \mu\text{M}$  and the culture then left to respire nitric oxide.

In the model, Equations (2, 7 & 9) are now involved, as the nitric oxide reductase NorB is being used in addition to the requirement to model the chemical inhibition of  $\text{cbb}_3$  by nitric oxide. The parameter posterior probability distributions generated from the Monte-Carlo runs from the oxygen reduction dataset were used as prior probability distributions for this next dataset. The unknown parameters (those not included in the previous dataset) were set to sensible non-zero values which would allow them to burn-in and generate subsequent posterior distributions. The datasets used for this section of the model describe the effect on oxygen reduction as nitric oxide is introduced to a system that is only partially primed for microaerobic respiration. There will be a small amount of NorB (the nitric oxide reductase) present to remove and nitric oxide that is present. The  $\text{nsrR}^-$  mutant, which expresses NorB in an essentially constitutive manner was not effective in generating a usable dataset as it removed any NO almost instan-

taneously resulting in an almost featureless dataset (data not shown).

The dataset and final solved output from the Monte-Carlo run are shown in figure 6.1. This is a more complex dataset than for oxygen respiration. Initially the oxygen reduction is carried out in exactly the same manner as the previous dataset, which is able to be modelled with the parameters selected from the prior distributions. Upon addition of nitric oxide, oxygen respiration slows and almost stops as a result of competition for electrons between  $cbb_3$  and NorB, and the direct chemical inhibition of  $cbb_3$  by NO. Nitric oxide starts being removed as a combination of simple diffusion (although this rate will be low) and reduction via NorB. Once the NO has been removed from the system oxygen reduction resumes at almost the same rate as before and still has the same high affinity feature as the previous dataset. The closeness of fit of the solved parameter set to the experimental data shows that the model has been able to accommodate a parameter set from the prior distributions that is able to accommodate all these features, and will still be able to model simple oxygen reduction.

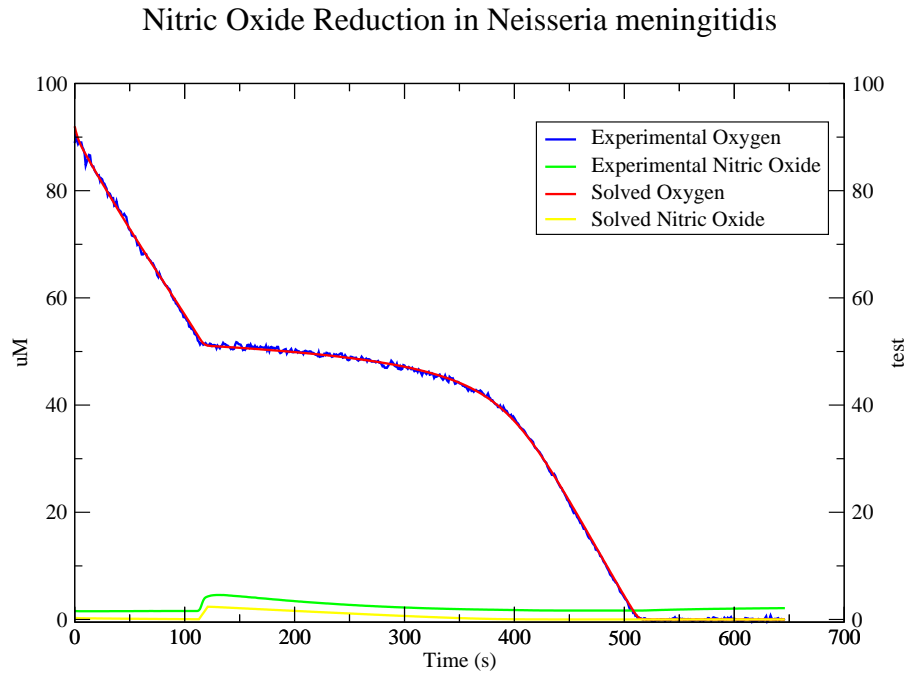


Figure 6.1: **Nitric Oxide Reduction in *Neisseria meningitidis*.** This dataset shows the effect on rate of oxygen reduction as nitric oxide is introduced to the system. The solved output, using prior probabilities from the oxygen reduction dataset show an almost perfect match to the features of the experimental dataset. The solved oxygen concentrations match the experimental dataset so closely as to be almost invisible.

## **6.1 Aerobic Nitric Oxide Reduction**

### **6.1.1 Introduction**

### **6.1.2 Results**

### **6.1.3 Discussion**

## **6.2 Microaerobic Nitric Oxide Reduction**

### **6.2.1 Introduction**

### **6.2.2 Results**

### **6.2.3 Discussion**

## **6.3 Aerobic Nitric Oxide Reduction in *nsrR*<sup>-</sup> mutant**

### **6.3.1 Introduction**

### **6.3.2 Results**

### **6.3.3 Discussion**

## Chapter 7

# Nitrite Reduction in *N. meningitidis*

Modelling nitrite reduction involves growing NsrR deficient cultures in aerobic conditions. This mutant expresses AniA and NorB in a constitutive manner, removing the necessity for growing the cultures in microaerobic conditions. The cultures are grown for 3-4 hours after which the culture is added to the electrode chamber and Sodium Nitrite added to a concentration of 1 mM.

In the model, Equations (3.3 & 3.8) are now also involved, allowing parametrisation of kinetic rates of AniA. This experimental dataset does not unfortunately describe how the concentration of NO changes while Nitrite is being reduced. The prior probability distributions used for this dataset were the posteriors generated from the Nitric Oxide Reduction dataset described above, in accordance with Bayesian inference. The unknown parameters were given non-zero values with flat priors, allowed to burn-in and were then used to generate posterior probability distributions.

A representative dataset and solved output is shown in figure 7.1.

This is a simpler dataset than for Nitric oxide reduction as it only describes nitrite reduction, along with a small change in oxygen concentration. In combination with prior probability distributions from the afore mentioned dataset it means that the possible values for the kinetic rates involved are automatically going to be limited to those that work alongside the given priors. Without the prior probability distributions the posterior distributions would have a similar

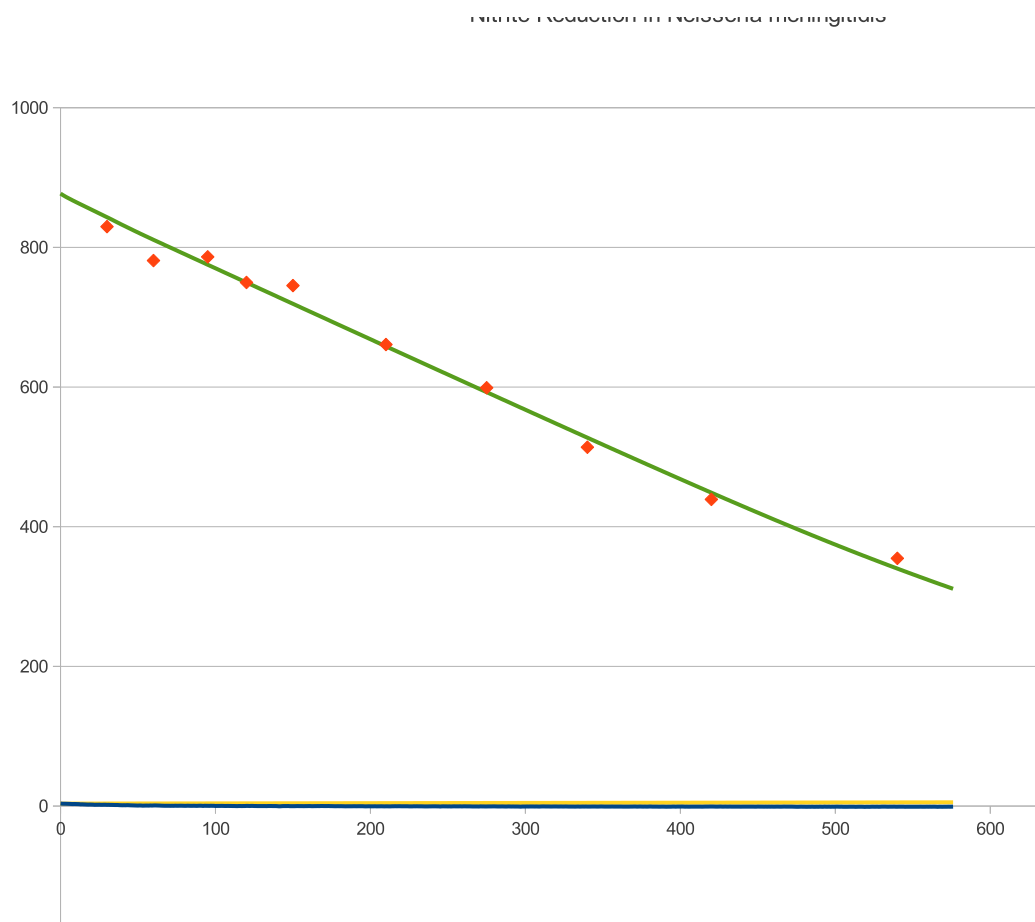


Figure 7.1: **Nitrite Reduction in *Neisseria meningitidis*.** This dataset shows the rate of nitrite reduction when cultures have been grown in microaerobic conditions. The concentrations of nitrite were measured off-line leading to discontinuous data, however the solved output closely matches the experimental data for nitrite.

outcome to that of the first dataset used, where simple oxygen reduction was modelled, i.e. very wide distributions.

## **7.1 Microaerobic Nitrite Reduction**

### **7.1.1 Introduction**

### **7.1.2 Results**

### **7.1.3 Discussion**

## **7.2 Microaerobic Nitrite Reduction in *norB*<sup>-</sup> mutant**

### **7.2.1 Introduction**

### **7.2.2 Results**

### **7.2.3 Discussion**

## **7.3 Aerobic Nitrite Reduction in *nsrR*<sup>-</sup> mutant**

### **7.3.1 Introduction**

### **7.3.2 Results**

### **7.3.3 Discussion**

## **7.4 Aerobic Nitrite Reduction in *nsrR*<sup>-</sup>-*norB*<sup>-</sup> mutant**

### **7.4.1 Introduction**

### **7.4.2 Results**

### **7.4.3 Discussion**



# Chapter 8

## AniA and NorB Expression in *N. meningitidis*

### 8.1 Aerobic and Microaerobic Expression

#### 8.1.1 Introduction

#### 8.1.2 Results

#### 8.1.3 Discussion

## **Chapter 9**

# **The Completed Model**

# Appendix A

## Appendix

$$\begin{aligned}\frac{d[O_2]}{dt} &= \beta \left(1 - \frac{[O_2]}{K_O}\right) - k_1[C_a][O_2] \\ \frac{d[NO]}{dt} &= m_1[NO_2^-][A_a] - l_1[NO][B_a] - k_5[C_a][NO] + k_6[C_X] - \gamma[NO] \\ \frac{d[NO_2^-]}{dt} &= -m_1[NO_2^-][A_a] \\ \frac{d[Q_a]}{dt} &= g([Q] - [Q_a]) - l_3[Q_a]([B] - [B_a]) - f[Q_a]([X] - [E]) \\ \frac{d[E]}{dt} &= -k_3([C] - [C_a] - [C_X])[E] - m_3([A] - [A_a])[E] + f[Q_a]([X] - [E]) \\ \frac{d[A_a]}{dt} &= m_3([A] - [A_a])[E] - m_1[NO_2^-][A_a] \\ \frac{d[B_a]}{dt} &= l_3[Q_a]([B] - [B_a]) - l_1[NO][B_a] \\ \frac{d[C_a]}{dt} &= k_3([C] - [C_a] - [C_X])[E] - k_1[C_a][O_2] - k_5[C_a][NO] \\ \frac{d[C_X]}{dt} &= k_5[C_a][NO] - k_6[C_X] \\ \frac{d[A]}{dt} &= \left( R \left(1 - \frac{[O_2] + k_{10}[NO]}{[O_2] + k_{10}[NO] + k_{11}}\right) - S \left(1 - \frac{[NO]}{[NO] + k_{13}}\right) \right) - k_8[A] \\ \frac{d[B]}{dt} &= T \left( \frac{[NO]}{[NO] + k_{15}} \right) - k_{16}[B]\end{aligned}\tag{A.1}$$

Symbol	Description
$O_2$	Oxygen concentration
$NO$	Nitric oxide concentration
$NO_2^-$	Nitrite concentration
$E$	Reduced cytochrome concentration
$A_a$	Reduced AniA
$B_a$	Reduced NorB
$C_a$	Reduced $cbb_3$
$C_X$	Reversibly inhibited $cbb_3$
$Q_a$	Reduced Quinones

Table A.1: Model Variables

Symbol	Description
$k_1$	Rate of $O_2$ reduction by reduced $cbb_3$
$k_3$	Rate of $cbb_3$ reduction by cytochrome pool
$l_1$	Rate of $NO$ reduction by reduced NorB
$l_3$	Rate of NorB reduction by quinone pool
$m_1$	Rate of $NO_2^-$ reduction by reduced AniA
$m_3$	Rate of AniA reduction by cytochrome pool
$k_5$	Rate of $cbb_3$ inhibition by $NO$
$k_6$	Rate of recovery of $NO$ inhibited $cbb_3$
$\beta$	Rate of passive diffusion in of $O_2$
$K_O$	Saturation $O_2$ level
$g$	Rate of electrons in from NADH
$f$	Rate of reduction of cytochromes by quinones
$\gamma$	Spontaneous loss of $NO$
$Q$	Concentration of quinones
$X$	Concentration of cytochromes
$A$	Concentration of AniA
$B$	Concentration of NorB
$C$	Concentration of $cbb_3$

Table A.2: Model Parameters

# List of Abbreviations

<b>AniA</b>	Anaerobically inducible protein A from <i>Neisseria</i> sp.
<b>ATP</b>	Adenosine triphosphate
<b>CAB</b>	Columbia Agar Base
<b>CFU</b>	Colony Forming Units
<b>CSF</b>	Cerebrospinal Fluid
<b>FNR</b>	Fumarate and Nitrite reduction Regulator
<b>HCO</b>	Haem Copper Oxidase
<b>LSD</b>	Least-Squares Difference
<b>MHB</b>	Müller-Hinton Broth
<b>NADH</b>	Nicotinamide adenine dinucleotide
<b>NarP</b>	Nitrate/Nitrite Response Regulator
<b>NarQ</b>	Nitrate/Nitrite Response Sensor
<b>NED</b>	<i>N</i> -1-naphthylethylenediamine dihydrochloride
<b>NOR</b>	Nitric Oxide Reductase
<b>NorB</b>	Nitric Oxide Reductase B from <i>Neisseria</i> sp.
<b>NsrR</b>	Nitrite sensing repressor protein
<b>OD</b>	Optical Density
<b>ODE</b>	Ordinary Differential Equation
<b>PDE</b>	Partial Differential Equation
<b>rpm</b>	Revolutions Per Minute
<b>spc<sup>r</sup></b>	Spectinomycin resistance
<b>tet<sup>r</sup></b>	Tetracyclin resistance

# References

1. van Deuren M, Brandtzaeg P, van der Meer JWM (2000) Update on Meningococcal Disease with Emphasis on Pathogenesis and Clinical Management. Clin Microbiol Rev 13: 144–166.
2. Stephens DS (2009) Biology and Pathogenesis of the Evolutionarily Successful, Obligate Human Bacterium *Neisseria meningitidis*. Vaccine 27: B71–B77.
3. Rosenstein NE, Perkins BA, Stephens DS, Popovic T, Hughes JM (2001) Meningococcal Disease. N Engl J Med 344: 1378–1388.
4. DeVoe IW (1982) The Meningococcus and Mechanisms of Pathogenicity. Microbiol Mol Biol Rev 46: 162–190.
5. Aas JA, Paster BJ, Stokes LN, Olsen I, Dewhirst FE (2005) Defining the Normal Bacterial Flora of the Oral Cavity. J Clin Microbiol 43: 5721–5732.
6. Madigan M, Martinko J, editors (2005) Brock Biology of Microorganisms. 11th ed., Prentice Hall.
7. Carbonnelle E, Hill DJ, Morand P, Griffiths NJ, Bourdoulous S, et al. (2009) Meningococcal Interactions with the Host. Vaccine 27: B78–B89.
8. Larson JA, Higashi DL, Stojiljkovic I, So M (2002) Replication of *Neisseria meningitidis* Within Epithelial Cells Requires TonB-Dependent Acquisition of Host Cell Iron. Infect Immun 70: 1461–1467.

9. Archibald FS, DeVoe IW (1978) Iron in *Neisseria meningitidis*: Minimum Requirements, Effects of Limitation, and Characteristics of Uptake. *J Bacteriol* 136: 35–48.
10. Perkins-Balding D, Ratliff-Griffin M, Stojiljkovic I (2004) Iron Transport Systems in *Neisseria meningitidis*. *Microbiol Mol Biol Rev* 68: 154–171.
11. Yazdankhah SP, Caugant DA (2004) *Neisseria meningitidis*: An Overview of the Carriage State. *J Med Microbiol* 53: 821–832.
12. Beddek AJ, Li MS, Kroll JS, Jordan TW, Martin DR (2009) Evidence for Capsule Switching between Carried and Disease-Causing *Neisseria meningitidis* Strains. *Infect Immun* 77: 2989–2994.
13. Moxon ER, Rainey PB, Nowak MA, Lenski RE (1994) Adaptive Evolution of Highly Mutable Loci in Pathogenic Bacteria. *Current Biology* 4: 24–33.
14. Pathan N, Faust SN, Levin M (2003) Pathophysiology of Meningococcal Meningitis and Septicaemia. *Arch Dis Child* 88: 601–607.
15. Exley RM, Shaw J, Mowe E, Sun YH, West NP, et al. (2005) Available Carbon Source Influences the Resistance of *Neisseria meningitidis* Against Complement. *J Exp Med* 201: 1637–1645.
16. Beno DW, Devine LF, Larson GL (1968) Identification of *Neisseria meningitidis* Carbohydrate Fermentation Patterns in Mueller-Hinton Broth. *J Bacteriol* 96: 563.
17. Rock JD, Mahnane MR, Anjum MF, Shaw JG, Read RC, et al. (2005) The Pathogen *Neisseria meningitidis* Requires Oxygen, but Supplements Growth by Denitrification. Nitrite, Nitric Oxide and Oxygen Control Respiratory Flux at Genetic and Metabolic Levels. *Mol Microbiol* 58: 800–9.
18. Rock JD, Moir JWB (2005) Microaerobic Denitrification in *Neisseria meningitidis*. *Biochem Soc Trans* 33: 134–6.

19. Tuttle DM, Scherp HW (1952) Studies On The Carbon Dioxide Requirement Of *Neisseria meningitidis*. J Bacteriol 64: 171–182.
20. Lundberg JO, Weitzberg E, Cole JA, Benjamin N (2004) Nitrate, Bacteria and Human Health. Nat Rev Micro 2: 593–602.
21. Deeudom M, Rock J, Moir J (2006) Organization of the Respiratory Chain of *Neisseria meningitidis*. Biochem Soc Trans 34: 139–42.
22. Deeudom M (2007) The Electron Transport Chains of *Neisseria meningitidis*. Ph.D. thesis, University of York.
23. Preisig O, Zufferey R, Thony-Meyer L, Appleby C, Hennecke H (1996) A High-affinity cbb3-Type Cytochrome Oxidase Terminates the Symbiosis-Specific Respiratory Chain of *Bradyrhizobium japonicum*. J Bacteriol 178: 1532–1538.
24. Brown GC, Cooper C (1994) Nanomolar Concentrations of Nitric Oxide Reversibly Inhibit Synaptosomal Respiration by Competing with Oxygen at Cytochrome Oxidase. FEBS Letters 356: 295–298.
25. Sharpe MA, Cooper CE (1998) Interaction of Peroxynitrite with Mitochondrial Cytochrome Oxidase. J Biol Chem 273: 30961–30972.
26. Anjum MF, Stevanin TM, Read RC, Moir JWB (2002) Nitric Oxide Metabolism in *Neisseria meningitidis*. J Bacteriol 184: 2987–2993.
27. Heurlier K, Thomson MJ, Aziz N, Moir JWB (2008) The Nitric Oxide (NO)-Sensing Repressor NsrR of *Neisseria meningitidis* has a Compact Regulon of Genes Involved in NO Synthesis and Detoxification. J Bacteriol 190: 2488–95.
28. Deeudom M, Koomey M, Moir JWB (2008) Roles of C-type Cytochromes in Respiration in *Neisseria meningitidis*. Microbiology 154: 2857–64.



29. Rock JD, Thomson MJ, Read RC, Moir JWB (2007) Regulation of Denitrification Genes in *Neisseria meningitidis* by Nitric Oxide and the Repressor NsrR. *J Bacteriol* 189: 1138–44.
30. Isabella V, Wright LF, Barth K, Spence JM, Grogan S, et al. (2008) Cis- and Trans-Acting Elements Involved in Regulation of NorB (NorZ), The Gene Encoding Nitric Oxide Reductase in *Neisseria gonorrhoeae*. *Microbiology* 154: 226–239.
31. Pitcher RS, Watmough NJ (2004) The Bacterial Cytochrome cbb3 Oxidases. *Biochimica et Biophysica Acta (BBA) - Bioenergetics* 1655: 388 – 399.
32. Puustinen A, Verkhovsky MI, Morgan JE, Belevich NP, Wikstrom M (1996) Reaction of the *Escherichia coli* Quinol Oxidase Cytochrome bo3 with Dioxygen: The Role of a Bound Ubiquinone Molecule. *Proc Natl Acad Sci U S A* 93: 1545–1548.
33. van der Oost J, de Boer AP, de Gier JW, Zumft WG, Stouthamer AH, et al. (1994) The Heme-Copper Oxidase Family Consists of Three Distinct Types of Terminal Oxidases and is Related to Nitric Oxide Reductase. *FEMS Microbiol Lett* 121: 1–9.
34. García-Horsman JA, Barquera B, Rumbley J, Ma J, Gennis RB (1994) The Superfamily of Heme-Copper Respiratory Oxidases. *J Bacteriol* 176: 5587–5600.
35. Keilin D, Hartree EF (1939) Cytochrome and Cytochrome Oxidase. *Proceedings of the Royal Society of London Series B, Biological Sciences* 127: pp. 167–191.
36. Huang Y, Reimann J, Singh LMR, Adelroth P (2010) Substrate Binding and the Catalytic Reactions in Cbb3-type Oxidases: The Lipid Membrane Modulates Ligand Binding. *Biochim Biophys Acta* 1797: 724–731.

37. Zufferey R, Preisig O, Hennecke H, ThÄny-Meyer L (1996) Assembly and Function of the Cytochrome cbb3 Oxidase Subunits in *Bradyrhizobium japonicum*. J Biol Chem 271: 9114–9119.
38. Preisig O, Zufferey R, Hennecke H (1996) The *Bradyrhizobium japonicum* fixGHIS Genes are Required for the Formation of the High-Affinity cbb3-type Cytochrome Oxidase. Arch Microbiol 165: 297–305.
39. Householder TC, Fozo EM, Cardinale JA, Clark VL (2000) Gonococcal Nitric Oxide Reductase is Encoded by a Single Gene, NorB, Which is Required for Anaerobic Growth and is Induced by Nitric Oxide. Infect Immun 68: 5241–5246.
40. Barth KR, Isabella VM, Clark VL (2009) Biochemical and Genomic Analysis of the Denitrification Pathway within the Genus *Neisseria*. Microbiology 155: 4093–4103.
41. Clark VL, Campbell LA, Palermo DA, Evans TM, Klimpel KW (1987) Induction and Repression of Outer Membrane Proteins by Anaerobic Growth of *Neisseria gonorrhoeae*. Infect Immun 55: 1359–1364.
42. Moir JW (2011) A Snapshot of a Pathogenic Bacterium Mid-evolution: *Neisseria meningitidis* is Becoming a Nitric Oxide-Tolerant Aerobe. Biochem Soc Trans 39: 1890–1894.
43. Weiss H, Friedrich T, Hofhaus G, Preis D (1991) The Respiratory-Chain NADH Dehydrogenase (Complex I) of Mitochondria. Eur J Biochem 197: 563–576.
44. Carroll J, Fearnley IM, Shannon RJ, Hirst J, Walker JE (2003) Analysis of the Subunit Composition of Complex I from Bovine Heart Mitochondria. Mol Cell Proteomics 2: 117–126.
45. Friedrich T, Böttcher B (2004) The Gross Structure of the Respiratory Complex I: a Lego System. Biochim Biophys Acta 1608: 1–9.

46. Yagi T (1991) Bacterial NADH-Quinone Oxidoreductases. *J Bioenerg Biomembr* 23: 211–225.
47. Gemperli AC, Dimroth P, Steuber J (2002) The Respiratory Complex I (NDH I) from *Klebsiella pneumoniae*, a Sodium Pump. *J Biol Chem* 277: 33811–33817.
48. Thöny-Meyer L (1997) Biogenesis of Respiratory Cytochromes in Bacteria. *Microbiology and Molecular Biology Reviews* 61: 337–76.
49. Darrouzet E, Valkova-Valchanova M, Ohnishi T, Daldal F (1999) Structure and Function of the Bacterial bc1 Complex: Domain Movement, Subunit Interactions, and Emerging Rationale Engineering Attempts. *J Bioenerg Biomembr* 31: 275–288.
50. Snyder CH, Gutierrez-Cirlos EB, Trumpower BL (2000) Evidence for a Concerted Mechanism of Ubiquinol Oxidation by the Cytochrome bc 1 Complex. *Journal of Biological Chemistry* 275: 13535–13541.
51. Berry EA, Huang LS (2011) Conformationally Linked Interaction in the Cytochrome bc(1) Complex Between Inhibitors of the Q(o) Site and the Rieske Iron-Sulfur Protein. *Biochim Biophys Acta* 1807: 1349–1363.
52. Crofts AR, Shinkarev VP, Kolling DRJ, Hong S (2003) The Modified Q-Cycle Explains the Apparent Mismatch Between the Kinetics of Reduction of Cytochromes c1 and bh in the bc1 Complex. *J Biol Chem* 278: 36191–36201.
53. Wood PM (1983) Why do c-type Cytochromes Exist? *FEBS Lett* 164: 223–226.
54. Ambler RP (1991) Sequence Variability in Bacterial Cytochromes c. *Biochim Biophys Acta* 1058: 42–47.

55. Chang HY, Ahn Y, Pace LA, Lin MT, Lin YH, et al. (2010) The Diheme Cytochrome C(4) from *Vibrio cholerae* is a Natural Electron Donor to the Respiratory cbb(3) Oxygen Reductase. *Biochemistry* 49: 7494–7503.
56. Clark VI, Isabella VM, Barth K, Overton TW (2010) Regulation and Function of the Neisserial Denitrification Pathway: Life with Limited Oxygen. In: Genco CA, Wetzler L, editors, *Neisseria: Molecular Mechanisms of Pathogenesis*, chap. 2, pp. 19–39, Caister Academic Press.
57. Edwards J, Cole LJ, Green JB, Thomson MJ, Wood AJ, et al. (2010) Binding to DNA Protects *Neisseria meningitidis* Fumarate and Nitrate Reductase Regulator (FNR) from Oxygen. *Journal of Biological Chemistry* 285: 1105–1112.
58. Overton TW, Whitehead R, Li Y, Snyder LAS, Saunders NJ, et al. (2006) Coordinated Regulation of the *Neisseria gonorrhoeae*-Truncated Denitrification Pathway by the Nitric Oxide-Sensitive Repressor, NsrR, and Nitrite-Insensitive NarQ-NarP. *J Biol Chem* 281: 33115–33126.
59. Baker SC, Ferguson SJ, Ludwig B, Page MD, Richter OM, et al. (1998) Molecular Genetics of the Genus *Paracoccus*: Metabolically Versatile Bacteria with Bioenergetic Flexibility. *Microbiol Mol Biol Rev* 62: 1046–1078.
60. Nicholls DG, Ferguson SJ (1992) *Bioenergetics* 3. 2nd ed., Academic Press.
61. Kahlem P, Birney E (2006) Dry Work in a Wet World: Computation in Systems Biology. *Mol Syst Biol* 2: 40.
62. Doyle FJr, Stelling J (2006) Systems Interface Biology. *J R Soc Interface* 3: 603–16.
63. Kitano H (2002) Computational Systems Biology. *Nature* 420: 206–10.
64. Kitano H (2002) Systems Biology: A Brief Overview. *Science* 295: 1662–4.

65. Valencia A, Pazos F (2002) Computational Methods for the Prediction of Protein Interactions. *Curr Opin Struct Biol* 12: 368–73.
66. Mündermann L, Erasmus Y, Lane B, Coen E, Prusinkiewicz P (2005) Quantitative Modeling of Arabidopsis Development. *Plant Physiol* 139: 960–8.
67. Prusinkiewicz P (2004) Modeling Plant Growth And Development. *Curr Opin Plant Biol* 7: 79–83.
68. Prusinkiewicz P, Rolland-Lagan AG (2006) Modeling Plant Morphogenesis. *Curr Opin Plant Biol* 9: 83–8.
69. Crampin EJ, Halstead M, Hunter P, Nielsen P, Noble D, et al. (2004) Computational Physiology and the Physiome Project. *Exp Physiol* 89: 1–26.
70. Barabási AL, Oltvai ZN (2004) Network Biology: Understanding the Cell's Functional Organization. *Nat Rev Genet* 5: 101–13.
71. Peercy BE, Cox SJ, Shalel-Levanon S, San KY, Bennett G (2006) A Kinetic Model of Oxygen Regulation of Cytochrome Production in *Escherichia coli*. *J Theor Biol* 242: 547–563.
72. Almeida JS, Reis MAM, Carrondo MJT (1997) A Unifying Kinetic Model of Denitrification. *Journal of Theoretical Biology* 186: 241–249.
73. Cavaliere M, Ardelean II (2006) Applications of Membrane Computing, chap. Modeling Respiration in Bacteria and Respiration/Photosynthesis Interaction in Cyanobacteria Using a P System Simulator, pp. 129–158. Springer.
74. Klipp E, Herwig R, Kowald A, Wierling C, Lehrach H (2005) Systems Biology in Practice. Concepts, Implementation and Application. WILEY-VCH Verlag GmbH & Co. KGaA, Weinheim.

75. Gillespie DT (1977) Exact Stochastic Simulation of Coupled Chemical Reactions. *The Journal of Physical Chemistry* 81: 2340–2361.
76. Sauro HM, Hucka M, Finney A, Wellock C, Bolouri H, et al. (2003) Next Generation Simulation Tools: The Systems Biology Workbench and BioSPICE Integration. *OMICS: A Journal of Integrative Biology* 7: 355–372.
77. Hoops S, Sahle S, Gauges R, Lee C, Pahle J, et al. (2006) COPASI—a COMplex PATHway Simulator. *Bioinformatics* 22: 3067–3074.
78. Radhakrishnan K, Hindmarsh AC (1993) Description and Use of LSODE, the Livermore Solver for Ordinary Differential Equations. Tech. rep., NASA.
79. Gibson MA, Bruck J (2000) Efficient Exact Stochastic Simulation of Chemical Systems with Many Species and Many Channels. *The Journal of Physical Chemistry A* 104: 1876–1889.
80. McGuinness B, Barlow AK, Clarke IN, Farley JE, Anilionis A, et al. (1990) Deduced Amino Acid Sequences of Class 1 Protein (Pora) from Three Strains of *Neisseria meningitidis*. Synthetic Peptides Define the Epitopes Responsible for Serosubtype Specificity. *J Exp Med* 171: 1871–1882.
81. Clark LC, Wolf R, Granger D, Taylor Z (1953) Continuous Recording of Blood Oxygen Tensions by Polarography. *Journal of Applied Physiology* 6: 189–193.
82. Liu X, Liu Q, Gupta E, Zorko N, Brownlee E, et al. (2005) Quantitative Measurements of NO Reaction Kinetics with a Clark-Type Electrode. *Nitric Oxide* 13: 68 – 77.
83. Bedioui F, Villeneuve N (2003) Electrochemical Nitric Oxide Sensors for Biological Samples: Principle, Selected Examples and Applications. *Electroanalysis* 15: 5–18.

84. Serpe MJ, Zhang X (2007) The Principles, Development and Application of Microelectrodes for the In Vivo Determination of Nitric Oxide. In: Michael AC, Borland LM, editors, *Electrochemical Methods for Neuroscience*, chap. 21, CRC Press.
85. Nicholas DJ, Nason A (1957) Determination of Nitrate and Nitrite. In: *Methods in Enzymology*, vol. 3, pp. 981–984, Academic Press.
86. Aga RG, Hughes MN (2008) The Preparation and Purification of NO Gas and the Use of NO Releasers: The Application of NO Donors and Other Agents of Nitrosative Stress in Biological Systems. In: Poole RK, editor, *Globins and Other Nitric Oxide-Reactive Proteins, Part A*, vol. 436 of *Methods in Enzymology*, pp. 35 – 48, Academic Press.
87. Cole LJ, Huston WM, Moir JWB (2008) Delivery of Nitric Oxide for Analysis of the Function of Cytochrome C'. In: Poole RK, editor, *Globins and Other Nitric Oxide-Reactive Proteins, Part A*, vol. 436 of *Methods in Enzymology*, pp. 21 – 33, Academic Press.
88. Giuffre A, Barone MC, Mastronicola D, D'Itri E, Sarti P, et al. (2000) Reaction of Nitric Oxide with the Turnover Intermediates of Cytochrome c Oxidase: Reaction Pathway and Functional Effects. *Biochemistry* 39: 15446–15453.
89. Forte E, Urbani A, Saraste M, Sarti P, Brunori M, et al. (2001) The Cytochrome cbb3 from *Pseudomonas stutzeri* Displays Nitric Oxide Reductase Activity. *Eur J Biochem* 268: 6486–6491.
90. Hunter H (2007) Characterisation of the Oxidase Activity in *Neisseria lactamica*.
91. Nojiri M, Koteishi H, Nakagami T, Kobayashi K, Inoue T, et al. (2009) Structural Basis of Inter-Protein Electron Transfer for Nitrite Reduction in Denitrification. *Nature* 462: 117–120.

92. Blackmore RS, Greenwood C, Gibson QH (1991) Studies of the Primary Oxygen Intermediate in the Reaction of Fully Reduced Cytochrome Oxidase. *Journal of Biological Chemistry* 266: 19245–9.
93. Hedrick DB, White DC (1986) Microbial Respiratory Quinones in the Environment: I. A Sensitive Liquid Chromatographic Method. *Journal of Microbiological Methods* 5: 243 – 254.
94. Butcher JC (2003) *Numerical Methods for Ordinary Differential Equations*. John Wiley and Sons.
95. Cash JR, Karp AH (1990) A Variable Order Runge-Kutta Method for Initial Value Problems with Rapidly Varying Right-hand Sides. *ACM Trans Math Softw* 16: 201–222.
96. Press WH, Teukolsky SA, Vetterling WT, Flannery BP (1992) *Numerical Recipes in C*. 2nd ed., Cambridge University Press.
97. Nakamura (Particle Data Group) K (2010) Review of Particle Physics. *Journal of Physics G: Nuclear and Particle Physics* 37: 075021 and 2011 partial update for the 2012 edition.
98. Kirkpatrick S, Gelatt CD, Vecchi MP (1983) Optimization by Simulated Annealing. *Science* 220: pp. 671–680.
99. Černý V (1985) Thermodynamical Approach to the Traveling Salesman Problem: An Efficient Simulation Algorithm. *Journal of Optimization Theory and Applications* 45: 41–51.
100. Bertsimas D, Tsitsiklis J (1993) Simulated Annealing. *Statistical Science* 8: pp. 10–15.
101. Toni T, Welch D, Strelkowa N, Ipsen A, Stumpf MPH (2009) Approximate Bayesian Computation Scheme for Parameter Inference and Model Selection in Dynamical Systems. *Journal of The Royal Society Interface* 6: 187.



102. Ronquist F, Teslenko M, van der Mark P, Ayres D, Darling A, et al. (2011) MrBayes 3.2: Efficient Bayesian Phylogenetic Inference and Model Choice Across a Large Model Space. *Systematic Biology* in press: 0–0.
103. Beaumont MA, Zhang W, Balding DJ (2002) Approximate Bayesian computation in population genetics. *Genetics* 162: 2025–2035.
104. Sisson SA, Fan Y, Tanaka MM (2007) Sequential Monte Carlo without likelihoods. *Proc Natl Acad Sci U S A* 104: 1760–1765.
105. Beaumont MA (2010) Approximate Bayesian Computation in Evolution and Ecology. *Annual Review of Ecology, Evolution, and Systematics* 41: pp. 379–406.
106. Metropolis N, Rosenbluth AW, Rosenbluth MN, Teller AH, Teller E (1953) Equation of State Calculations by Fast Computing Machines. *The Journal of Chemical Physics* 21: 1087–1092.
107. Hastings WK (1970) Monte Carlo Sampling Methods Using Markov Chains and Their Applications. *Biometrika* 57: 97–109.